Cenozoic Shortening and Propagation in the Eastern Kuqa Fold-And-Thrust Belt, South Tian Shan, NW China

Feng Li, Xiaogan Cheng, Hanlin Chen, Xuhua Shi, Yong Li, Julien Charreau, Ray Weldon

Tectonics

RESEARCH ARTICLE
10.1029/2022TC007447

Cenozoic Shortening and Propagation in the Eastern Kuqa Fold-And-Thrust Belt, South Tian Shan, NW China

Feng Li[1,2], Xiaogan Cheng[1,2], Hanlin Chen[1,2], Xuhua Shi[1,2,3], Yong Li[4], Julien Charreau[5], and Ray Weldon[6]

[1]Key Laboratory of Geoscience Big Data and Deep Resource of Zhejiang Province, School of Earth Sciences, Zhejiang University, Hangzhou, China, [2]Research Center for Structures in Oil and Gas Bearing Basins, Ministry of Education, Hangzhou, China, [3]Xinjiang Pamir Intracontinental Subduction National Observation and Research Station, Beijing, China, [4]Research Institute of Petroleum Exploration and Development, PetroChina Tarim Oilfield Company, Korla, China, [5]CRPG, CNRS, UMR 7358, Université de Lorraine, Vandœuvre-lès-Nancy, France, [6]Department of Earth Sciences, University of Oregon, Eugene, OR, USA

Abstract In an orogen-foreland basin system, syn-orogenic sedimentation and deformation records within the foreland basin provide critical evidence for understanding uplift and erosion processes of adjacent orogenic belts. Foreland fold-and-thrust belts (FTBs) are widely developed around the Tian Shan range, Central Asia. Problem of how crustal shortening accumulates and propagates from the Tian Shan to adjacent foreland basins is essential for understanding the overall dynamics of Tian Shan. In this study, we interpreted three high-resolution seismic reflection profiles to estimate the magnitude and distribution of Cenozoic shortening across the Eastern Kuqa FTB, South Tian Shan foreland. Combined with well-dated syntectonic stratigraphy, we further evaluate the timing, rate, and migration of the deformation front of the Kuqa FTB. Our results suggest that the Kuqa FTB's total crustal shortening increases westward. The distribution of crustal shortening across secondary structural belts shows a gradual, basinward decrease, which can be explained by the telescoped mechanism. Propagation rates of the Kuqa FTB's deformation front indicate an episodic propagation of the foreland thrust wedge, with an acceleration after ~12 Ma. Similar episodic propagation pattern has also been observed in other foreland FTBs around the Tian Shan, but they show significant spatio-temporal variations in the propagation stages and related rates.

Plain Language Summary The Tian Shan range stretches over 2,500 km from east to west and is one of the Earth's largest intracontinental orogenic belts. As the mountains grew, deformation propagated into foreland basins around the range, forming a series of fold-and-thrust belts (FTBs). To better understand the spatial distribution of crustal shortening, and basinward propagation process in foreland FTBs, we interpret and reconstruct three high-resolution seismic profiles across the Eastern Kuqa FTB, South Tian Shan. Our study indicates that the total crustal shortening of the Eastern Kuqa FTB increases westward. Within the Kuqa FTB, a telescoped distribution pattern of crustal shortening is also observed in frontal thin-skinned structures above the regional salt décollements. In addition, we find that the basinward propagation of Kuqa FTB is episodic, which is featured by a two-stage evolution pattern.

Key Points:

- The Eastern Kuqa fold-and-thrust belt shows a westerly increase in total shortening and a telescoped pattern in shortening distribution
- The Cenozoic propagation of the Kuqa thrust belt indicates an episodic process that accelerated after ~12 Ma
- Basinward growth of the Tian Shan orogenic wedge varies spatiotemporally; propagation stages and rates vary in different foreland basins

Supporting Information:

Supporting Information may be found in the online version of this article.

Correspondence to:

H. Chen and X. Shi,
hlchen@zju.edu.cn;
shixuhua@zju.edu.cn

Citation:

Li, F., Cheng, X., Chen, H., Shi, X., Li, Y., Charreau, J., & Weldon, R. (2023). Cenozoic shortening and propagation in the Eastern Kuqa fold-and-thrust belt, South Tian Shan, NW China. *Tectonics*, *42*, e2022TC007447. https://doi.org/10.1029/2022TC007447

Received 6 JUN 2022
Accepted 6 MAY 2023

Author Contributions:

Conceptualization: Feng Li, Xiaogan Cheng, Xuhua Shi, Julien Charreau
Formal analysis: Feng Li
Funding acquisition: Xiaogan Cheng, Hanlin Chen, Xuhua Shi
Investigation: Xiaogan Cheng, Hanlin Chen, Xuhua Shi, Yong Li
Methodology: Feng Li, Xiaogan Cheng, Xuhua Shi, Julien Charreau
Project Administration: Xiaogan Cheng, Hanlin Chen, Xuhua Shi

1. Introduction

The India-Eurasia collision caused the uplift of the Tibetan Plateau and extensive intracontinental deformation over a broad area of Asia during the Cenozoic. Located more than 1,000–2,000 km to the north of this collision zone, the 2,500-km-long Tian Shan, with numerous peaks over 7,000 m, is a seismically active orogenic belt and has experienced Cenozoic tectonic reactivation and rapid uplift since the Miocene (Avouac & Tapponnier, 1993; Bullen et al., 2003; Molnar & Tapponnier, 1975; Sobel et al., 2006; Tapponnier & Molnar, 1979). The uplift of the Tian Shan has affected the geosystem in at least two aspects. On one hand, the significant topography of the Tian Shan has played a key role in the climate evolution of Central Asia since the Late Miocene (Charreau et al., 2009; Miao et al., 2012; Prud'Homme et al., 2021; Sun et al., 2015); on the other hand, the deformation propagated and disrupted adjacent foreland basins, resulting in the development of a series of fold-and-thrust belts (FTBs) that encode key deformational and erosional records of the Tian Shan (Figure 1). GPS velocity field indicates that the Western Tian Shan accommodates nearly 40% of the present-day total convergence between Indian and Eurasia plates (Abdrakhmatov et al., 1996; Reigber et al., 2001; Q. Wang et al., 2001). Moreover, at

Resources: Xiaogan Cheng, Hanlin Chen, Xuhua Shi, Yong Li, Julien Charreau
Supervision: Xiaogan Cheng, Hanlin Chen, Xuhua Shi, Julien Charreau
Writing – original draft: Feng Li, Xuhua Shi
Writing – review & editing: Feng Li, Xiaogan Cheng, Hanlin Chen, Xuhua Shi, Yong Li, Julien Charreau, Ray Weldon

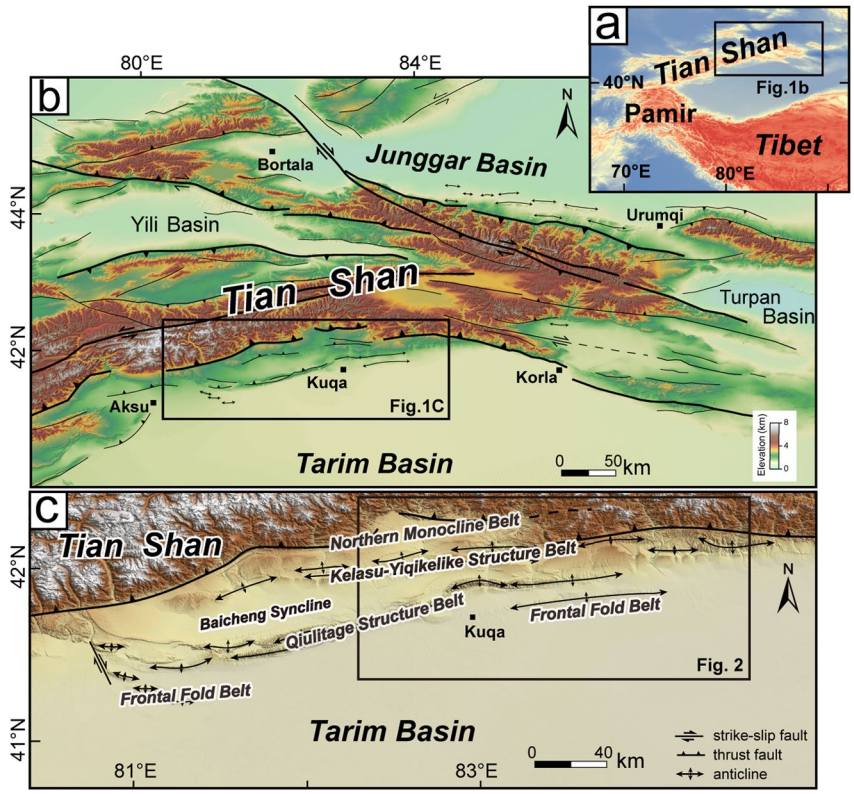

Figure 1. Topography and tectonic setting of the study region. (a) Shaded relief map of Central Asia, showing the location of the Tian Shan. (b) Topographic map of the Eastern Tian Shan orogenic belt and adjacent regions; the black rectangle shows the location of the Kuqa fold-and-thrust belt (FTB). (c) Shaded relief map of the Kuqa fold-and-thrust belt, showing five major tectonic units. The Eastern Kuqa FTB is shown within the black rectangle.

the northern and southern edges of the Tian Shan, 80%–90% of the current N-S shortening is absorbed by the foreland FTBs (S. Yang, Li, & Wang, 2008). However, due to the spatial diversity of foreland basins, how this massive shortening accumulated and propagated within the orogen-basin system remains unclear, and is critical for the understanding of the outward growth of the Tian Shan and related continental tectonics in central Asia.

Considerable effort has been made in recent decades to quantify the crustal shortening and development sequence of the FTBs around the Tian Shan foreland basins (Abdulhameed et al., 2020; Allen et al., 1999; Burchfiel et al., 1999; Chang et al., 2019; Heermance et al., 2008; H. Lu et al., 2010; Scharer et al., 2004; Thompson Jobe et al., 2018; X. Wang et al., 2011; X. Yang, Deng, et al., 2008; M. Yang et al., 2010; Yin et al., 1998; Yu et al., 2014). However, limited by subsurface seismic profile quality and relatively few deformation age constraints of multiple faults and anticlines in the past, few studies explore the spatiotemporal distribution pattern of the shortening, basinward propagation of deformation front and related mechanisms (Goode et al., 2014; Heermance et al., 2008; H. Lu et al., 2010; Thompson Jobe et al., 2018). In the Kuqa FTB, southern Tian Shan piedmont, over 10 km-thick Meso-Cenozoic strata were deposited and deformed during the late Cenozoic (X. Wang et al., 2011). Previous studies mainly focused on the FTB's deformation style (Izquierdo-Llavall et al., 2018; S. Li et al., 2012, 2013; Neng et al., 2018; Qi et al., 2009; X. Wang et al., 2011; W. Wang et al., 2017; Z. Wu et al., 2014), lateral structural variation (Pla et al., 2019; W. Wang et al., 2020; Z. Zhang et al., 2019), and thermochronological constraints on the regional uplift and exhumation history within FTB (Chang et al., 2017; Dumitru et al., 2001; W. Yang et al., 2017; Yu et al., 2014). Moreover, based on geological mapping and reconstruction of cross sections, a few other studies also calculated the crustal shortening of the Kuqa FTB, indicating a westward increase of the regional crustal shortening (Burchfiel et al., 1999; Izquierdo-Llavall et al., 2018; S. Li et al., 2012; L. Lu, Sun, et al., 2019; X. Wang et al., 2011; X. Yang, Deng, et al., 2008). Recent works also focused on a fold-scale deformation history and landscape evolution. Examples include the evolution of detachment folds within the Frontal fold belt of the Kuqa FTB (Gao et al., 2020; Hubert-ferrari et al., 2007; L. Lu, Sun, et al., 2019;

Tian et al., 2016), geomorphological analysis and fold modeling of the Misikantage, Yaken, and Qiulitage anticlines (Adeoti & Webb, 2022; Charreau et al., 2020; Daëron et al., 2007; Delcaillau et al., 2021; Saint-carlier et al., 2016; Tang et al., 2017; L. Zhang et al., 2021) and magnetostratigraphic studies of strata within active anticlines (Charreau et al., 2006, 2009; Sun et al., 2009; T. Zhang et al., 2014; Z. Zhang et al., 2016, 2018). Despite these efforts, the distribution and propagation of the shortening into the foreland basin and what mechanisms drive this process within the Kuqa FTB remain poorly understood.

To address these issues, we interpreted three high-resolution seismic reflection profiles across the Eastern Kuqa FTB, where major structural belts are prominent and well preserved (Figure 2). Along cross-sections, we use line length restoration and excess area methods to quantify the crustal shortening of each structural belt. Then, combined with the initial ages of individual faults and anticlines, we analyzed both distributions of crustal shortening and the basinward propagation of the deformation into the Eastern Kuqa FTB. Finally, combined with existing data on Cenozoic shortening and propagation of other FTBs around the Tian Shan, we further discuss the mechanism and spatio-temporal variation in basinward deformation around the Tian Shan.

2. Geological Setting

2.1. Structural Setting

The EW-striking Kuqa FTB is located in the southeastern piedmont of the Tian Shan, with a length of 400 km and a width of 30–80 km (Figures 1 and 2). Driven by regional N-S tectonic compression, large-scale thrusts and folds developed along the Kuqa foreland. Based on their tectonic styles and relative positions, the Kuqa FTB could be divided into five secondary structural belts: the northern monocline belt (NMB), Kelasu-Yiqikelike structural belt (KYSB), Baicheng syncline, Qiulitage structural belt (QLSB), and the Frontal fold belt (X. Wang et al., 2011). The NMB developed adjacent to the South Tian Shan thrust (STST) and is dominated by a series of basement-involved thrust faults. Recent published thermochronological data on these basement-involved faults indicated that regional uplift and deformation started between 42 and 36 Ma (Chang et al., 2017; Du et al., 2007; Yu et al., 2014). To the south, the KYSB is a highly deformed belt with several nearly E-W thrusts and folds

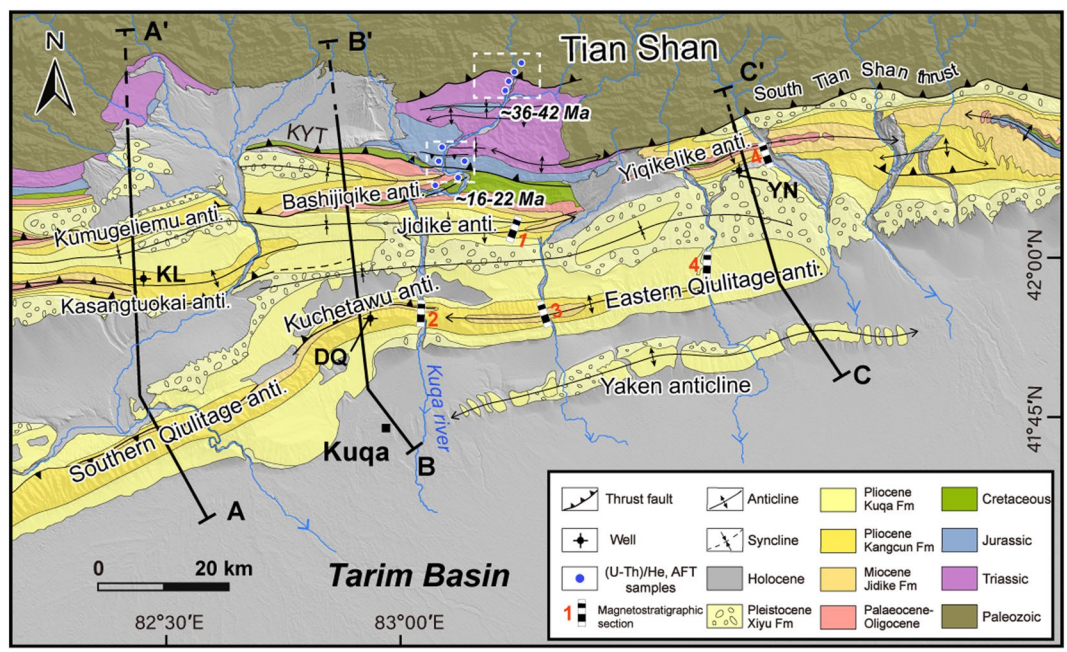

Figure 2. Geological map of the Eastern Kuqa fold-and-thrust belt, modified and simplified from X. Wang et al. (2011). Lines A-A', B-B', and C-C' show cross-sections discussed in this study: solid lines for segments with seismic reflection profiles, and dashed lines for sections interpreted by surface geology. Magnetostratigraphic sections addressed in the text include: 1-B. Huang et al. (2006); 2-Sun et al. (2009); 3-Charreau et al. (2006, 2009); 4-T. Zhang et al. (2014). The deformation ages of the South Tian Shan Thrust and Kelasu-Yiqikelike thrust are labeled. The ages are constrained through apatite fission track analysis and apatite (U-Th)/He dating (details in Chang et al., 2017; Yu et al., 2014).

(e.g., the Kumugeliemu, Kasangtuokai, Jidike, and Yiqikelike anticlines, etc., Figure 2). The Baicheng syncline is a gentle symmetric syncline involving thick late Cenozoic syntectonic sediments. The ~300-km-long arcuate QLSB, characterized by salt-cored detachment folds (S. Li et al., 2012), is the largest fold belt within the Kuqa FTB (Figure 1). Magnetostratigraphic studies of growth strata within the Kuchetawu and Eastern Qiulitage anticlines suggest that the folding of this belt began at ~6.5 Ma (Sun et al., 2009; T. Zhang et al., 2014). To the southernmost edge of the Kuqa FTB, the Frontal fold belt is comprised of a series of low amplitude and gentle detachment folds. It mainly includes the *en echelon* Kalayuergun anticlines in the west and the Yaken anticlines in the east. Recent magnetostratigraphic study of the Kalayuergun folds, modeling and area-depth-strain (ADS) analysis of seismic lines across the Yaken anticline suggest that they initiated around 5.5–5.3 Ma (Daëron et al., 2007; Gao et al., 2020; Hubert-ferrari et al., 2007; Z. Zhang et al., 2018).

2.2. Stratigraphy

Over 10 km-thick Meso-Cenozoic continental clastic rocks were deposited above the Paleozoic basement (Neng et al., 2018; X. Wang et al., 2011). The Mesozoic strata are mainly sand-shale sedimentary sequences (Figure 3), consisting of sandstone, siltstone and shale. In particular, coal-bearing layers are developed in the Upper Triassic to the Middle and Lower Jurassic strata, which form the lower basal décollement of the Kuqa FTB (Hendrix et al., 1992; Neng et al., 2018; X. Wang et al., 2011). Moreover, regional isopach maps also indicate that the thickness of Mesozoic strata decreases to the south, and the depocenter is located in the hinterland of the Kuqa FTB (X. Wang et al., 2011). The lower part of the Cenozoic stratigraphy is comprised of gypsum-salt layers of the Paleocene-Eocene Kumugelimu Formation (E_{1-2} km) and the Early Miocene Jidike Formation (N_1j), overlying the fluvial and alluvial detrital sequences (Izquierdo-Llavall et al., 2018). The salt sequences mainly consist of the Paleocene-Eocene Kumugeliemu group (E_{1-2} km) and early Miocene Jidike formation (N_1j). These two plastic salt-bearing strata are the upper décollements but the main décollement layer changes in different regions. The Western Kuqa FTB's main décollement layer is the Kumugeliemu gypsum-salt layers, while in the Eastern Kuqa FTB, the dominant décollement layer is the Jidike salt layers (S. Li et al., 2012; X. Wang et al., 2011). The overlying fluvial and alluvial detrital sequences mainly include the Kangcun (N_1k), Kuqa (N_2k), and Xiyu (Q_1x) formations. Based on published paleomagnetic studies in the Eastern Kuqa FTB, the magnetostratigraphic boundary ages of N_1j, N_1k, N_2k, and Q_1x are ~36, 13–9.8, 6.5–5.3, and 2.6–1.7 Ma (e.g., Charreau et al., 2006; B. Huang et al., 2006; Sun et al., 2009; T. Zhang et al., 2014).

3. Materials and Methods

Seismic reflection profiles and observed strata geometries, together with attributed ages of the sedimentary units, are commonly used in FTBs to constrain crustal shortening and deformation propagation. To better quantify the spatial distribution of crustal shortening and basinward propagation process of the Kuqa FTB, here we analyze three high-resolution 2D depth-converted, 50–90 km long seismic reflection profiles (Figures 4–6 and Figure S1 in Supporting Information S1), provided by the Tarim Oilfield Company, PetroChina. These seismic profiles were collected during 2010–2015, which are 30–40 km apart from west to east along the Eastern Kuqa FTB (Figure 2). In addition, we also used three wells (YN2, DQ8, and KL) data to calibrate stratigraphic reflector layers of seismic profiles.

The crustal shortening is estimated by section-balancing and restoration techniques. These methods are widely applied to calculate the shortening of contractional deformation in orogenic belts (Dahlstrom, 1969; Ghani et al., 2021; Hossack, 1979; Zuza et al., 2016). We used the structural modeling software *StructureSolver* (https://www.structuresolver.com) to help conduct palinspastic reconstruction for these sections (Figures 7–9). In particular, we adopted the fault parallel flow algorithm and followed the line length conservation for the reconstruction. Given the intense denudation of hanging wall strata, possible bed length changes during deformation and some unconstrained shortening in the pre-Cenozoic strata, our balanced cross sections provide a minimum magnitude of Cenozoic shortening. There are five key assumptions and/or limitations in our balancing reconstruction and shortening calculations: (a) Deformation is a plane strain within the north-south cross sections. We only reconstructed basic shortening amounts across 2D seismic profiles. (b) As the original thickness of the salt layers has changed significantly due to viscous flow during deformation, we restored the layers according to the thickness trends of the counterpart strata in the adjacent regions (K. Huang et al., 2020; S. Li et al., 2012). (c) We used the basal Tertiary (E_{1-2} km) layer as a common reference horizon to calculate the crustal shortening because it is the

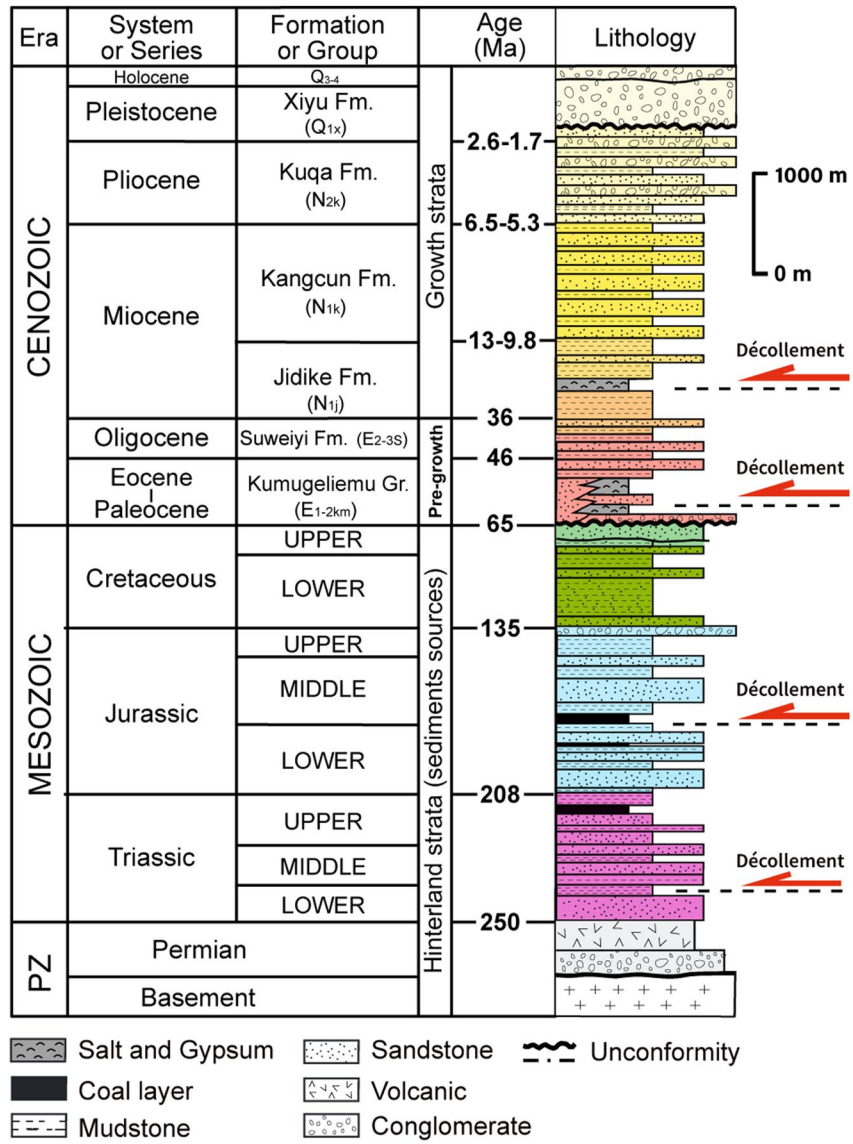

Figure 3. Synthesis stratigraphic column for the Kuqa fold-and-thrust belt (FTB) (modified and simplified after S. Li et al. (2012), Neng et al. (2018) and Pla et al. (2019)). PZ—Paleozoic. Note the growth and pre-growth strata, the two plastic salt-bearing strata, the Paleocene-Eocene Kumugeliemu Group (E_{1-2} km) and the Miocene Jidike Formation (N_1j), are the main regional décollements of the Kuqa FTB.

lowest Cenozoic strata, and shows clear high-amplitude reflectors within the seismic profiles (Figures 4–6). We restored this layer to a horizontal state, which is indicated by the parallel to the subparallel, low-angle unconformity between the Cretaceous and Tertiary strata. (d) The pin lines are placed at the relatively undeformed southernmost edge of the Kuqa FTB. And minimum fault offsets were used in restorations when the hanging wall cutoffs were eroded (Zuza et al., 2016). (e) To estimate the shortening distribution across each secondary structural belt (i.e., the NMB, Kelasu-Yiqikelike, Qiulitage, and Frontal fold belts), we calculated line length changes of each segment, assuming the bed's original length did not change during the folding process (Chamberlin, 1910; Dahlstrom, 1969; Wiltschko & Groshong, 2012).

Another approach for determining shortening across detachment folds in the Frontal fold belt of the Kuqa FTB is the ADS method (Groshong, 2015). This method follows area conservation along the analyzed cross-section above the décollement. In this study, we calculated each traced reflector horizon's excess area and related height (depth) above the interpreted décollement (Table S1 in Supporting Information S1). The shortening of the traced horizons could be calculated from the best-fit line of the related excess area-depth graph. Moreover, for the

pre-growth strata of a growth fold, the excess area-depth plot usually shows a linear trend. In contrast, for the growth strata within the same fold, the gradient decreased upward, indicating that the younger beds went through a less shortening (Epard & Groshong, 1993; Gonzalez-Mieres & Suppe, 2006, 2011). The deformation ages of individual structures are constrained by the recognition of growth strata in seismic profiles and published paleomagnetic ages of the Cenozoic strata within the Eastern Kuqa (Figure 2). Moreover, in the hinterland of the Kuqa FTB, where syn-tectonic strata have been strongly denuded, low-temperature thermochronology data (Chang et al., 2017; Du et al., 2007; Yu et al., 2014) were also used to constrain deformation ages of major bounding faults (i.e., STST fault and Kelasu-Yiqikelike thrust (KYT) fault).

4. Structures and Cenozoic Shortening of the Eastern Kuqa Fold-And-Thrust Belt

4.1. Structural Analysis of Seismic Profiles

4.1.1. Profile A-A'

The westernmost profile is the ~87 km long N-S seismic reflection profile A-A'. It runs through all four linear structural belts of the Kuqa FTB (i.e., the NMB, Kelasu-Yiqikelike, Qiulitage, and front folding structural belts, Figure 2). The upper part of the seismic profile is characterized by well-defined, continuous seismic reflectors of the late Cenozoic sedimentary strata. The Paleogene Kumugeliem Group is especially imaged between two regional, well-defined high-amplitude reflectors, and chaotic reflectors within the cores of anticlines along the profile indicate the flow of this plastic salt layer. To the northern part of this cross section, regional deformation of the NMB is characterized by the KYT. On the hanging wall of the fault, reflections are less continuous and the Mesozoic and Tertiary strata uplifted to the surface, forming a large syncline structure. The Kumugeliemu and Kasangtuokai anticlines compose the KYSB. These folds developed in the hanging wall of thrust faults, displaying a fault-propagation geometry (Figures 2 and 4). Moreover, the growth strata of these two anticlines indicate that the Kumugeliemu and Kasangtuokai anticlines began to develop in the early and late Miocene (N_1j and N_1k), respectively. The deep structure is complicated beneath the salt layer of the Paleogene Kumugeliem Group (E_{1-2} km, a high-amplitude unit marked by blue triangles in Figure 4a). Beneath the Kumugeliemu Group, small-scale thrusts and related anticlines developed along the lower décollements of Jurassic and Triassic strata.

The south end of the seismic profile imaged the QLSB and the Frontal fold belt. The southern Qiulitage anticline is nearly symmetric with gently dipping parallel seismic reflectors of both fold limbs. Massive salt and gypsum strata (chaotic reflectors within the core) filled the core of the anticlines during fold growth. Moreover, as imaged by the seismic profile, a south-dipping high-angle reverse fault and a minor back thrust also developed on the crest of this anticline (Figure 4b). Farther to the south, the Frontal fold belt is characterized by a detachment fold (Figures 4a and 4d). The fold is a buried structure with no apparent topographic expression on the ground surface.

4.1.2. Profiles B-B' and C-C'

The ~75-km long seismic profile B-B' is located ~40 km to the east of profile A-A' (Figure 2). Similarly, in the NMB of this section, the structure is dominated by north-dipping high-angle basement-involved thrust faults (Figure 5). Adjacent to the NMB, the Bashijiqike and Kasangtuokai anticlines comprise the KYSB within this section. The Bashijiqike anticline developed in the hanging wall of a north-dipping basement-involved thrust fault. In addition, a secondary thrust fault cuts upward through the strata within the core of this fold (Figures 5b and 5c). Adjacent to the Bashijiqike anticline, the Kasangtuokai anticline is interpreted as a fault-bend fold, whose lower detachment fault is in the coal and shale layers of the Triassic-Jurassic strata, while the upper detachment fault is in the gypsum-salt layers of the Jidike formation. Growth strata are well preserved in fold limbs of both Bashijiqike and Kasangtuokai anticlines. And the younger growth strata of the Kangcun formation (N_1k) within fold limbs of the Kasangtuokai anticline suggest that it developed later than the Bashijiqike anticline (Figure 5c). To the south, the QLSB is characterized by the Kuchetawu anticline. It grows above gypsum décollement layers of the Neogene Jidike formation (N_1j) and is mainly characterized by a south-dipping back thrust (Figure 5b). Similarly, a buried detachment fold with a slightly tilted décollement layer also developed in the southernmost of this seismic profile (Figure 5d).

Seismic reflection profile C-C' is ~53 km long and located at the eastern end of the Kuqa FTB (Figure 2). The deformation of the NMB gradually weakens to the east and disappears in this section, so this section only runs through the other three structural belts to the south. The KYSB is characterized by the Yiqikelike anticline

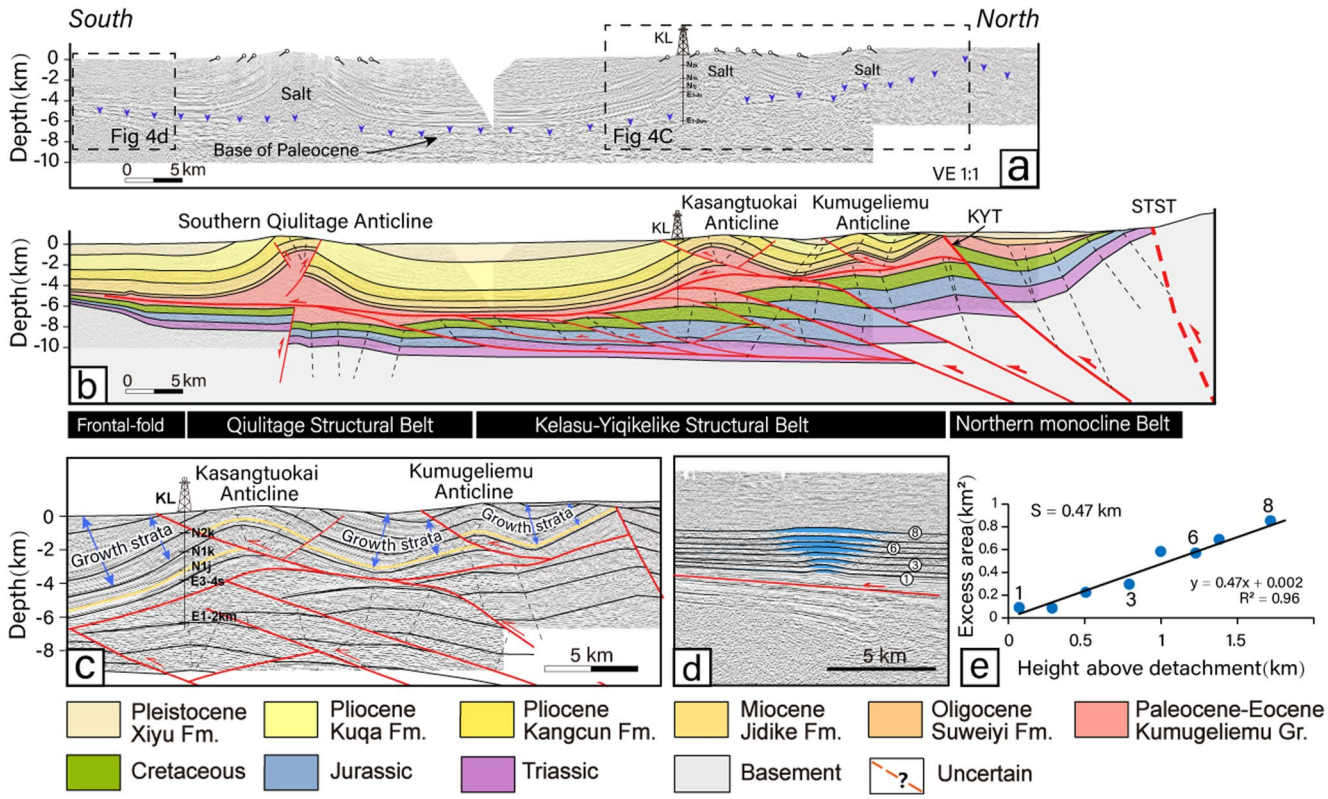

Figure 4. Interpreted seismic reflection profile A-A' and shortening estimate for the detachment fold within the Front fold belt. (a) Uninterpreted depth seismic profile A-A' (see Figure 2 for location); high-resolution figures are shown in Figure S1 in Supporting Information S1. The stratigraphy was constrained by the well KL and local surface geology. Blue triangles mark the bottom of the Paleocene Kumugeliem Group (E_{1-2} km), which serves as a regional décollement layer. (b) Geological interpretation of the seismic profile A-A'. (c) Enlarged detail from part of seismic reflection profile A-A'. Growth strata developed on both the Kumugeliemu and Kasangtuokai Anticline flanks, indicating that the Kumugeliemu anticline mainly initiated in the early Miocene (N_{1j}). In contrast, the Kasangtuokai Anticline developed during the late Miocene (N_{1k}). (d) Interpretation of the buried detachment fold. Depth above the detachment and area above the regional level is computed for each horizon. (e) The resultant area-depth (height) graph of the blind detachment fold.

southward of the South Tian Shan fault (Figure 6b). This fold is controlled by a thrust fault detached along the Triassic strata, we interpreted it as a breakthrough fault-propagation fold. Underneath the Yiqikelike anticline, a basement-involved thrust fault developed in deeper basement layers, which further amplifies the Yiqikelike anticline (Figure 6b). To the south, the asymmetric Eastern Qiulitage anticline developed. It is dominated by a low-angle north-dipping thrust fault, thrusting southward above the décollement along the Neogene Jidike formation (N_1j). Beneath the Jidike décollement, a south-verging thrust developed. This deep fault climbs up section from the lower décollement (the Jurassic coal layers) to the upper décollement in the evaporite layers of the Miocene Jidike formation (X. Wang et al., 2011). Farther to the south, the eastern edge of the Yaken anticline developed above a ~4.5 km deep décollement of the Miocene Jidike formation.

4.2. Cenozoic Shortening of the Eastern Kuqa FTB

Balanced cross section A-A' shows that the minimum total crustal shortening within the section is 26.3 ± 5.0 km, resulting in a shortening strain of 23% ± 4% (Figure 7, Table 1), as described in detail below. Cenozoic shortening across the NMB is difficult to constrain because of the denudation of Meso-Cenozoic strata (Figures 2 and 4). Based on the line-length balance of preserved Triassic strata and fault displacement of the KYT, we obtained a minimum shortening of ~1.7 and ~1.1 km, respectively. Shortening estimates across the STST fault are based on the thickness of preserved footwall strata and fault dip. At least ~2 km of footwall Mesozoic strata were cut by the STST fault, thus we place a minimum surface uplift of 2 km on the hanging wall of the STST fault. This vertical uplift combined with fault dip (30°–40°) of the STST fault along the southern Tian Shan range (Allen et al., 1999; Heermance et al., 2008; C. Y. Wu et al., 2019; Yin et al., 1998), provide a minimum horizontal shortening of

2.4 ± 1 km across the STST fault. These estimates yield a total minimum shortening of 5.2 ± 1 km across the NMB. To the south, more than half of the total shortening (~15.4 ± 3 km) occurred in the KYSB. The ~3 km of potential shortening error is from possible changes in subsurface fault geometry and present erosion surface of Kasangtuokai and Kumugeliemu anticlines (as in McQuarrie et al. (2008)). Further south, the minimum shortening of the QLSB is 5.2 ± 1 km. For the detachment fold of the Frontal fold belt, we traced eight seismic horizons for ADS analysis (Figures 4d and 4e). The obtained area-depth graph shows a prominent linear relationship ($R^2 = 0.96$), suggesting a shortening of ~0.5 km.

The total horizontal shortening of section B-B' is 20.9 ± 4.6 km, yielding a shortening strain of 17% ± 4% (Figure 8, Table 1). Both subsurface seismic profile and surface outcrops show that most Meso-Cenozoic strata have been eroded in the NMB (Figures 2 and 5). Line-length balance of preserved Triassic strata in this region yields a minimum shortening of ~1.6 km. Based on >3 km of regional exhumation suggested by recent low temperature thermochronology (Yu et al., 2014) and fault dip (30°–40°), we calculate a minimum shortening of 3.6 ± 1.6 km across the STST fault. These two estimates yield a total minimum shortening of 5.2 ± 1.6 km across the NMB. To the south, the minimum shortening of the KYSB is 11.1 ± 2 km, possible changes in fault geometry beneath the Kasangtuokai anticline can produce fault displacement error of ~2 km. Across the QLSB, the minimum shortening across the Kuchetawu anticline is 4.2 ± 1 km. For the detachment fold at the Frontal fold belt, we carefully traced 11 seismic horizons above the décollement for ADS analysis (Figure 5d). The excess area-depth plot reflects two separate groups (horizons 1–6 and 7–11). Linear regression between horizons 1 to 6 indicates a constant shortening of ~0.4 km. Notably, the excess area decreases upward from horizons 7 to 11, indicating that fold developed after the deposition of horizon 7.

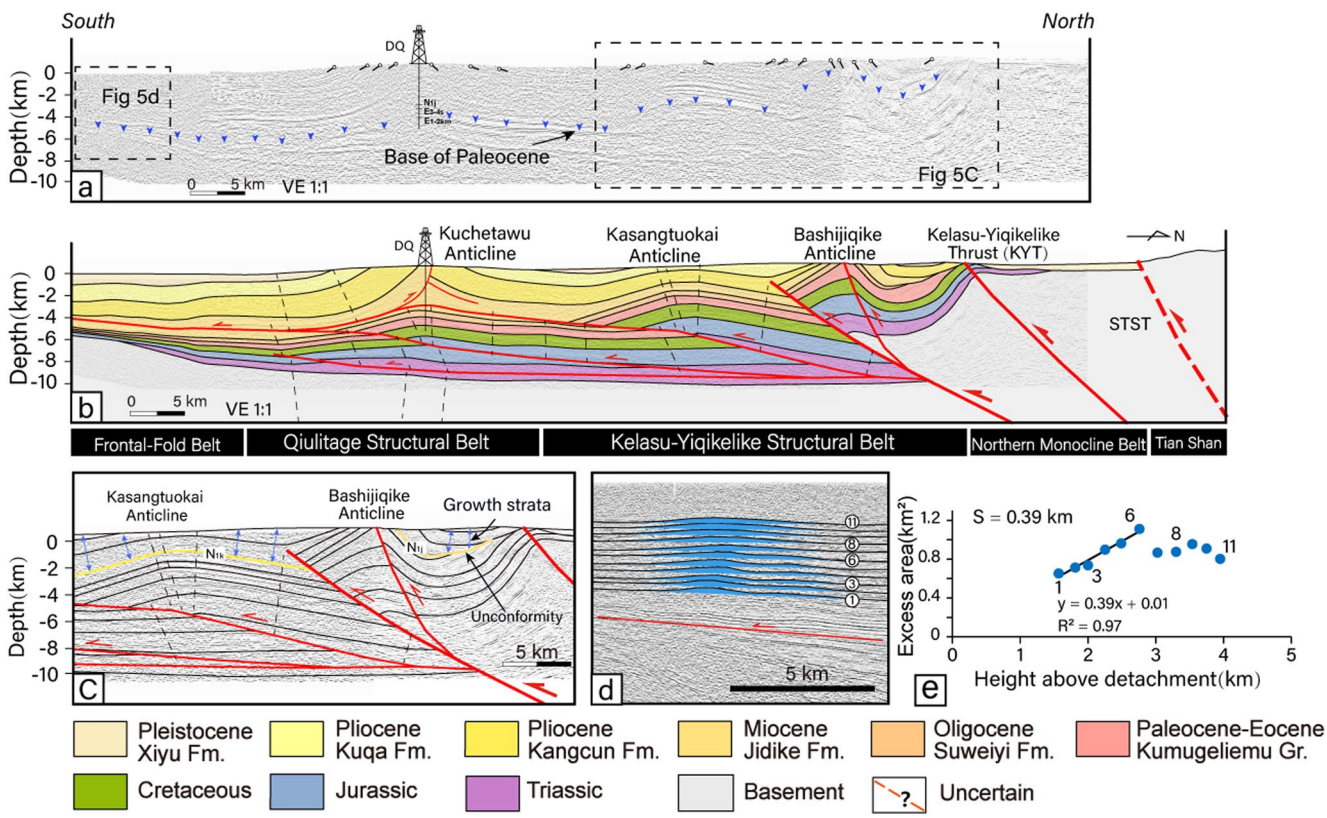

Figure 5. Interpreted seismic reflection profile B-B' and shortening estimate for the detachment fold within the Frontal fold belt. (a) Uninterpreted depth seismic profile B-B' (see location in Figure 2); high-resolution figure is shown in Figure S1 in Supporting Information S1. The stratigraphy was constrained by the well DQ and local surface geology. Black triangles mark the bottom of the Paleocene Kumugeliem Group (E_{1-2} km). (b) Geological interpretation of the seismic profile B-B'. (c) Enlarged detail from part of seismic reflection profile B-B', showing unconformities and growth strata developed in synclines. Growth strata show that the Bashijiqike Anticline initiated mainly in the early Miocene (N_1j), while the Kasangtuokai Anticline began to shorten in the late Miocene (N_1k). (d) Interpretation of the buried detachment fold. Depth above the detachment and area above the regional level is computed for each horizon. (e) The obtained area-depth (height) plot of the detachment fold. Horizons 1–6 show a best fit linear regression. However, the excess area decreases upward after horizon 7.

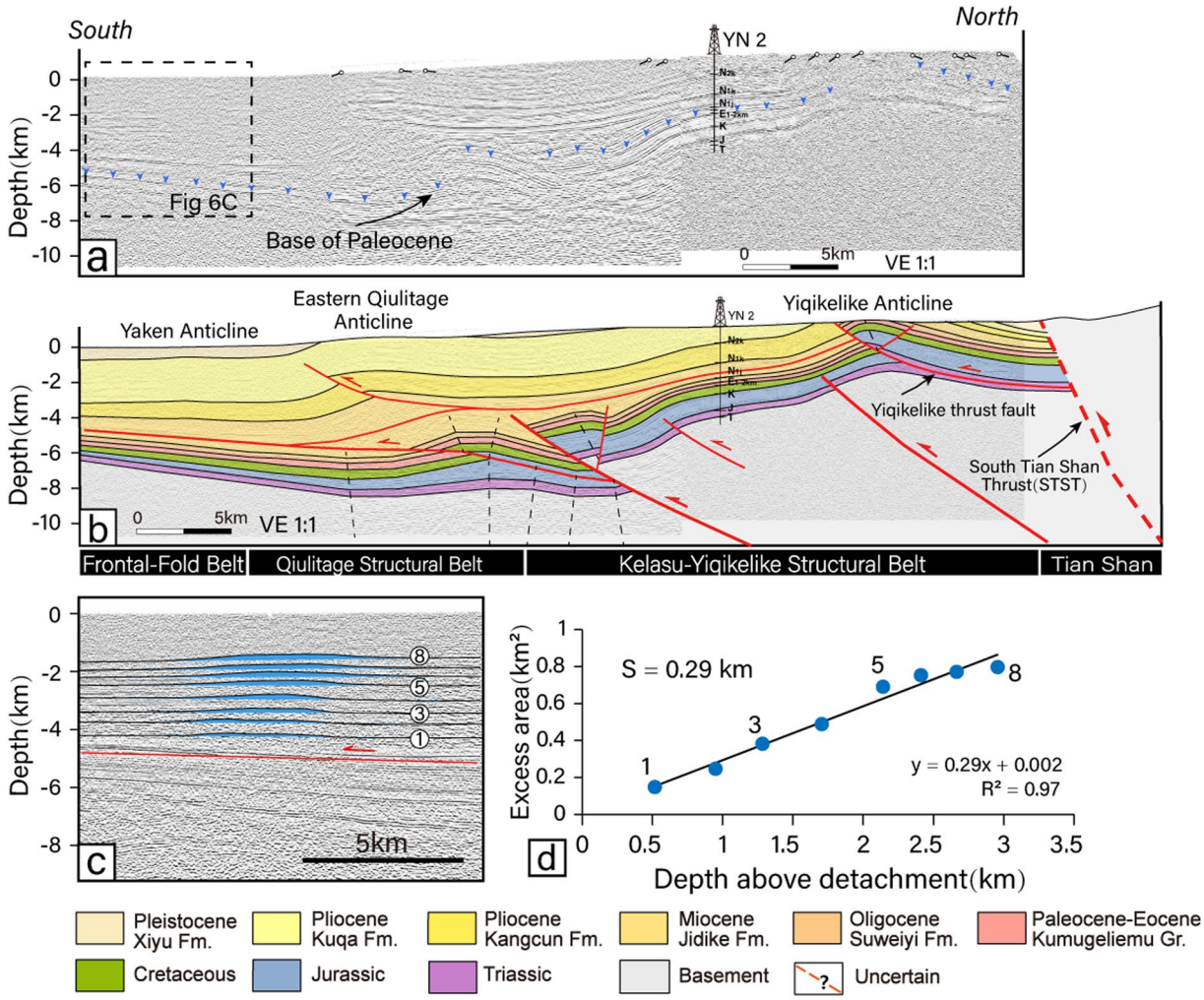

Figure 6. Interpreted seismic reflection profile C-C' and shortening estimate for the detachment fold within the Front fold belt. (a) Uninterpreted depth seismic profile C-C' (see location in Figure 2); high-resolution figure is shown in Figure S1 in Supporting Information S1. Stratigraphy is constrained by the well YN2 and local surface geology. Black triangles mark the bottom of the Paleocene Kumugeliem Group (E_{1-2} km). (b) Geological interpretation of the seismic profile C-C'. (c) Line drawing of the Yaken detachment fold. The distance above the detachment and the area above the regional level is computed for each horizon. (d) The obtained area-depth (height) plot of the detachment fold.

The restoration of section C-C' shows a total shortening of 11.1 ± 0.9 km, yielding a shortening strain of 17% ± 1% (Figure 9, Table 1). The NMB disappears in this section, and the Yiqikelike anticline developed adjacent to the STST fault. The minimum shortening across the KYSB is 6.9 ± 0.3 km, local seismic reflector distortions in the fault zone of the Yiqikelike thrust fault produced ~0.3 km of fault displacement error (Figure 6 and Figure S1 in Supporting Information S1). To the south, crustal shortening of the QLSB is accumulated by the eastern Qiulitage anticline in section C-C', and the minimum shortening of this anticline is 3.9 ± 0.6 km. To calculate shortening of the Yaken anticline to the south, we traced eight seismic horizons for the ADS analysis (Figure 6d); the area-depth graph indicates a prominent linear relationship ($R^2 = 0.97$) and a shortening of ~0.3 km. This value is smaller than ~1.2 km of shortening across the Yaken anticline to the west of the fold (Hubert-ferrari et al., 2007). This along-strike variation is mainly caused by the lateral growth of the Yaken anticline (Hubert-ferrari et al., 2007; Saint-carlier et al., 2016), which is also widely observed in the other active anticlines of the Kuqa FTB (Adeoti & Webb, 2022; Delcaillau et al., 2021; L. Zhang et al., 2021).

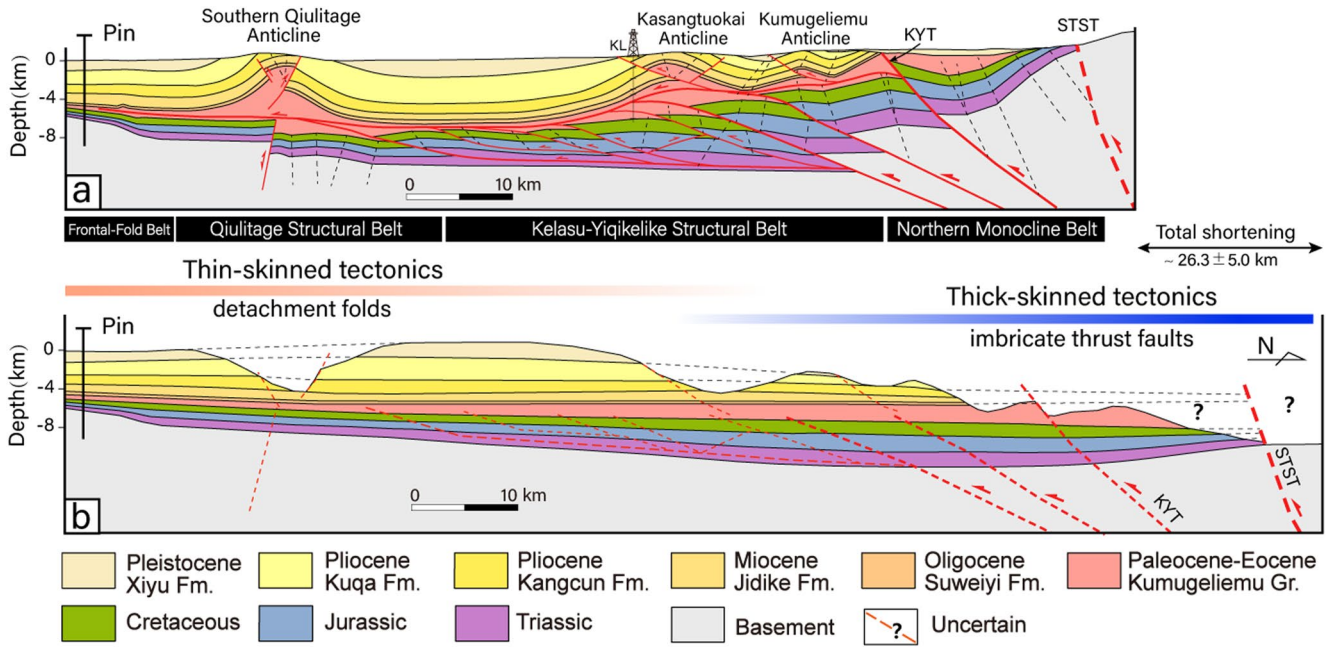

Figure 7. Regional geologic and balanced cross section A-A' within the Eastern Kuqa FTB. (a) Geological cross-section A-A' (see Figure 2 for location). (b) Restored cross section A-A'. We placed the pin line to the relatively undeformed southernmost edge of the section. STST: South Tian Shan Thrust.

5. Discussion

5.1. Spatial Patterns and Associated Mechanisms of Cenozoic Shortening Across the Eastern Kuqa Fold-And-Thrust Belt

Along the strike of the Eastern Kuqa FTB, results of three restored cross sections suggest that the total crustal shortening decreases eastward from 26.3 ± 5 km (section A-A') to 11.1 ± 0.9 km (section C-C') in the east. Our results complement several previous analyses of crustal shortening along the southern Tian Shan foreland (Allen et al., 1999; Burchfiel et al., 1999; Heermance et al., 2008; Izquierdo-Llavall et al., 2018; S. Li et al., 2012; Scharer et al., 2004; Tian et al., 2016; Yin et al., 1998; T. Zhang et al., 2014), which suggest an eastward decreasing trend of intracontinental deformation between the Southern Tian Shan and the Tarim craton block. This E-W strain gradient could be partly explained by the clockwise rotation of the Tarim block relative to the Junggar and Kazakhstan blocks (Avouac et al., 1993; Zubovich et al., 2010). In addition, the late Cenozoic convergence between the Pamir and western Tian Shan also contributed to this eastward decrease (Qiao et al., 2017; Thompson et al., 2015; Tian et al., 2016). Within the Eastern Kuqa FTB, accumulated shortening of both Kelasu-Yiqikelike

Table 1
Shortening Estimates From the Balanced Cross Sections

Structural belt	Cross section A-A'		Cross section B-B'		Cross section C-C'	
	Shortening (km)	Shortening strain (%)	Shortening (km)	Shortening strain (%)	Shortening (km)	Shortening strain (%)
Northern Monocline Belt (NMB)	5.2 ± 1	22 ± 4	5.2 ± 1.6	22 ± 6	N.D.	N.D.
Kelasu-Yiqikelike Structural Belt (KYSB)	15.4 ± 3	27 ± 5	11.1 ± 2	27 ± 5	6.9 ± 0.3	20 ± 1
Qiulitage Structural Belt (QLSB)	5.2 ± 1	19 ± 4	4.2 ± 1	14 ± 4	3.9 ± 0.6	21 ± 3
Front Fold Belt (FFB)	0.5	4	0.4	3	0.3	3
Totals	26.3 ± 5.0	23 ± 4	20.9 ± 4.6	17 ± 4	11.1 ± 0.9	17 ± 1

Note. See Figure 2 for section locations. Percent shortening is the shortening amount divided by the original length of the related structural belt (Present length + Shortening). Shortening errors are described within the text. N.D., no data.

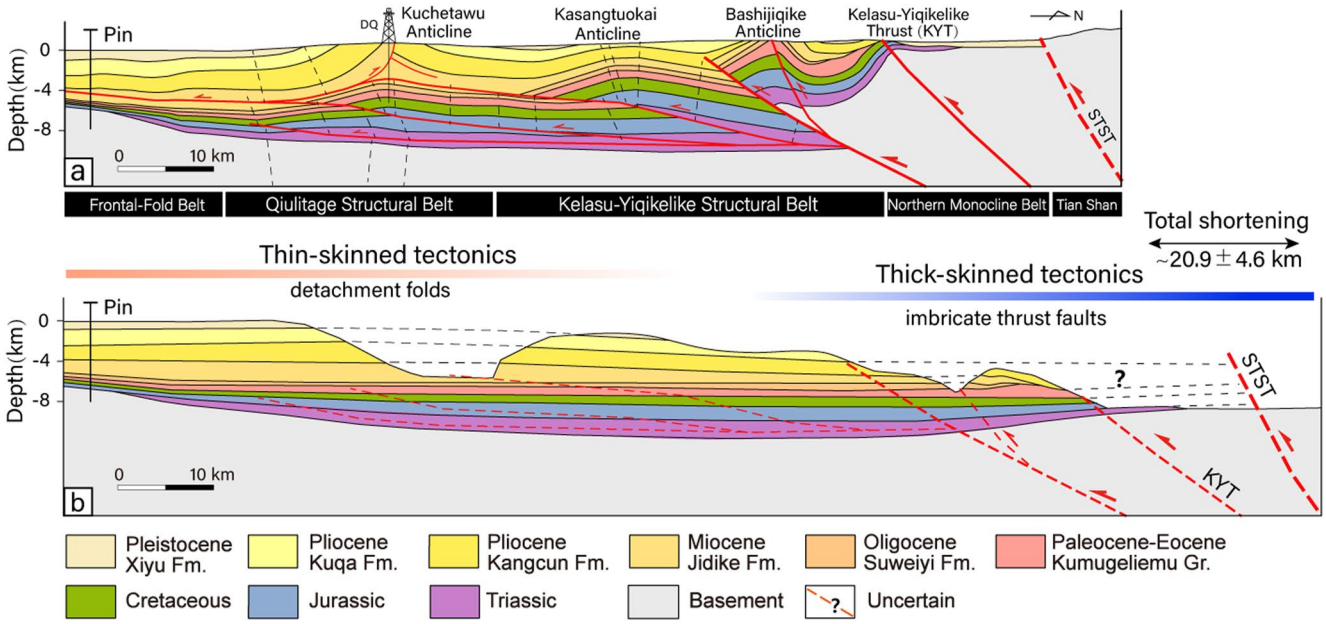

Figure 8. Regional geologic and balanced cross section B-B' within the Eastern Kuqa FTB. (a) Geologic cross-section B-B' (see Figure 2 for location). (b) Restored cross section B-B'. Most Meso-Cenozoic strata have been eroded in the northern monocline belt, line-length restoration using the preserved Triassic strata in this region.

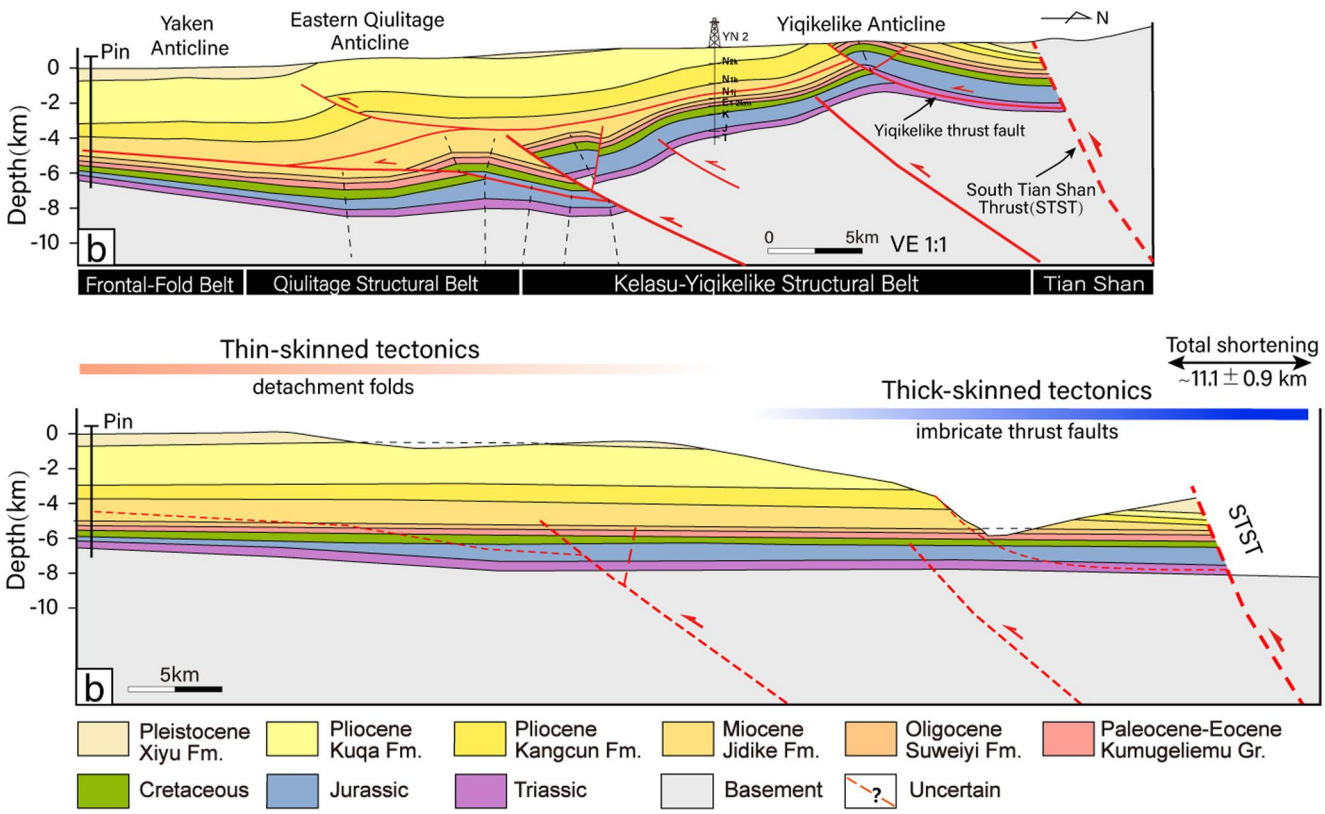

Figure 9. Regional geologic and balanced cross section C-C' within the Eastern Kuqa fold-and-thrust belt. (a) Geologic cross-section C-C' (see Figure 2 for location). The northern monocline belt disappears in this section, and the Yiqikelike anticline developed adjacent to the South Tian Shan thrust fault. (b) Restored cross section C-C'.

and QLSBs also show an obvious eastward decreasing trend (Table 1). However, the situation is different in the Frontal Fold belt, which is composed of several active anticlines and is widely regarded as the current deformation front of the Kuqa FTB (Daëron et al., 2007; Hubert-ferrari et al., 2007; Saint-carlier et al., 2016). Due to lateral growth of the fold, shortening reduces to both terminations. For instance, the shortening across the Yaken anticline decreases from ~1.2 km in its central segment (Hubert-ferrari et al., 2007) to 0.3–0.5 km (this study) in the eastern and western segments.

Across the strike of the Eastern Kuqa FTB, the distribution of crustal shortening shows a gradual, basinward decrease. The KYSB accumulated the maximum crustal shortening (6.9–15.4 km). Regional crustal shortening decreases further to 3.9–5.2 km at the QLSB. At the southernmost end of the Eastern Kuqa FTB, crustal shortening across detachment folds of the Frontal fold belt is only 0.3–1.2 km (Figures 4–6). This across-strike distribution mechanism can be regarded as a telescoping pattern, which widely developed in the foreland FTBs around the world (Boyer & Elliott, 1982; Meigs, 1997; Qayyum et al., 2015; Watkins et al., 2017). And the regional décollement of the Kuqa FTB mainly controls the above spatial distribution pattern. During the development of the Kuqa FTB, Cenozoic shortening is accommodated by a series of internal structures (i.e., thrusts, pop-ups and salt-cored anticlines) above the regional décollement (salt strata of Kumugeliemu group or Jidike formation). As deformation propagated along the décollement, early-developed structures could accumulate greater crustal shortening than the late-developed structures (Figure 10). Similar distribution pattern has also been observed in southwestern and the northern Tian Shan forelands. Although the locus of maximum shortening varied along the strike, from hinterland structures to the distal detachment folds, the distribution of crustal shortening also has a basinward decreasing tendency (Heermance et al., 2008; H. Lu et al., 2010; H. Lu, Li, et al., 2019; Scharer et al., 2004).

5.2. Basinward Propagation of the Kuqa FTB

5.2.1. Propagation of the Deformation Front

The propagation process of the foreland deformation front can provide indirect evidence to understand the building history of the adjacent orogenic belt (Avouac, 2003; Heermance et al., 2008; Simoes & Avouac, 2006; Thompson Jobe et al., 2018). In this study, we focused on this propagation process in the Eastern Kuqa FTB, where the regional temporal framework is well established by detailed paleomagnetic and thermochronologic ages (Chang et al., 2017; Charreau et al., 2006, 2009; Du et al., 2007; B. Huang et al., 2006; Sun et al., 2009; Yu et al., 2014; T. Zhang et al., 2014; Z. Zhang et al., 2015). The southward younging of uplift and exhumation

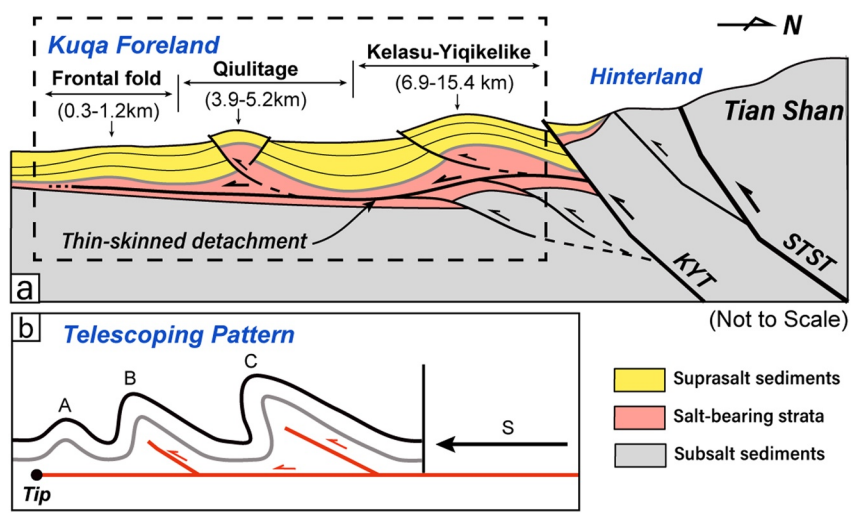

Figure 10. Schematic diagram showing displacement distribution (with a telescoping pattern) and distribution of shortening in the Eastern Kuqa fold-and-thrust belt (FTB). (a) Crustal shortening decreases from the Kelasu-Yiqikelike structural belt to the Front fold belt across the Eastern Kuqa FTB (see text for discussion). (b) The telescoping model was modified after Qayyum et al. (2015), demonstrating that crustal shortening in the telescoped wedge gradually decreases to zero at the tip of its basal detachment. Displacement amount: $A < B < C$, net total displacement $S = A + B + C$.

of structures within the Eastern Kuqa FTB through time, suggests that shortening gradually propagates from the South Tian Shan to the Tarim Basin during the late Cenozoic (Figure 11, Table 2). Based on initiation ages of secondary structural units within the Kuqa FTB, this sequential development and propagation of deformation could be divided into four stages. During stage 1, uplift on the STST and development of basement-involved faults in the NMB occurred after 42-36 Ma. During stage 2, displacement along the KYT fault, growth of anticlines and associated thrusting within the KYSB, developed from 22–16 Ma to 13–9.8 Ma. During stage 3, deformation of Qiulitage anticlines occurred after ~6.5 Ma. During stage 4, shortening across the Frontal fold belt and a series of detachment folds developed after 5.5–5.3 Ma.

Our palinspastic reconstruction of A-A' and B-B' sections, combined with temporal constraints on specific structures within the Eastern Kuqa FTB further enabled us to calculate the basinward propagation rates during different periods (Figures 11 and 12). Between 42–36 and 22–16 Ma (stage 1), the deformation front propagated from the STST to the KYT. These two faults are currently 23–17 km apart, they must have been a greater distance apart before the crustal shortening. Thus, adding 3.6–2.4 km of minimum shortening across the STST fault and ~1.6 km of minimum shortening across the NMB, the deformation front migrated 28.2–21.0 km over ~20 million years, yielding a propagation rate of 1.4–1.0 mm/yr. During stage 2, the deformation front further migrated to the southern boundary of the KYSB at 13–9.8 Ma (Figure 12a). The Kasangtuokai anticline is now 20.5–18.6 km away from the KYT. Combined with the minimum shortening of 15.4–11.1 km across the KYSB, the deformation front propagated 35.9–29.7 km over 9.0–6.2 million years, leading to a rapid propagation rate of 3.3–5.8 mm/yr. During stage 3, the deformation front migrated from the Kasangtuokai anticline to the southern Qiulitage and Kuqatawu anticlines. These two anticlines are located today some 19.2 and 15.3 km south of the Kasangtuokai anticline respectively, adding 5.2–4.2 km of shortening across them, the deformation front migrated 24.4–19.5 km over 6.5–3.3 million years, resulting in a propagation rate of 3–7.4 mm/yr. During stage 4, the deformation front propagated to Yaken anticline and other detachment folds at 5.5–5.3 Ma. The minimum propagation distance of this period is 13.8–9.6 km, yielding a propagation rate of 8–13.8 mm/yr. After ~5.3 Ma, the propagation of the deformation front seems to slow down. The southernmost end of seismic profiles shows no obvious deformation except for the shortening of detachment folds along the Frontal fold belt. The propagation rate may gradually decrease to zero (Figure 12b). Collectively, our analyses suggest an in-sequence, episodic process of overall deformation propagation of the Kuqa FTB during early Miocene to Holocene time with a two to three-fold increase in propagation rates since middle Miocene (Figure 12b).

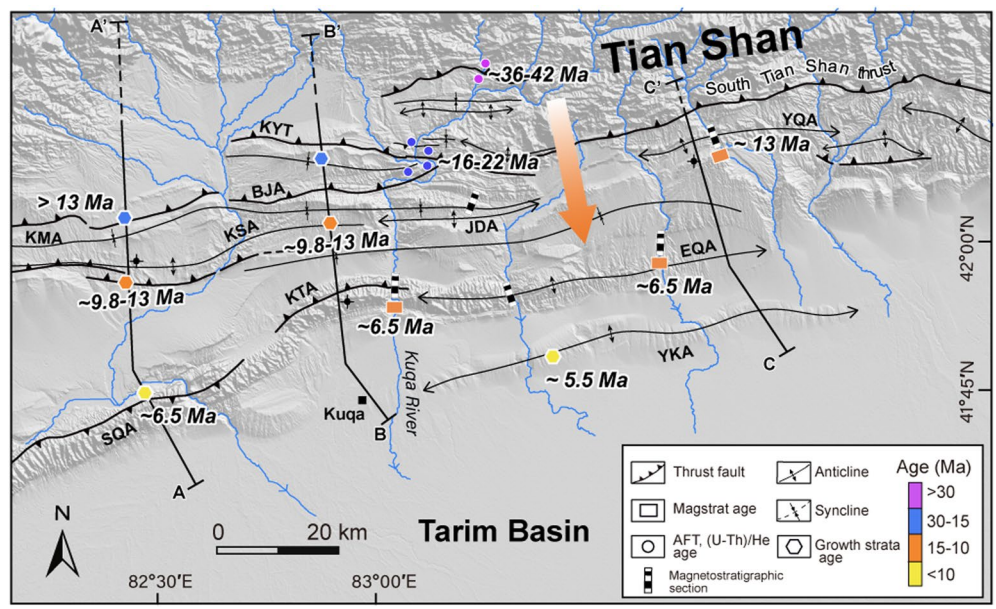

Figure 11. Interpreted initiation ages of different structures within the Eastern Kuqa fold-and-thrust belt illustrate basinward propagation of the Tian Shan front. Data from Charreau et al. (2006, 2009), B. Huang et al. (2006), Sun et al. (2009), T. Zhang et al. (2014), Yu et al. (2014), Chang et al. (2017). BJA, Bashijiqike Anticline; BYA, Biyoulebaoguzi Anticline; EQA, Eastern Qiutitag anticline; KMA, Kumugeliemu Anticline; KSA, Kasangtuokai Anticline; KTA, Kuqatawu Anticline; KYT, Kelasu-Yiqikelike Thrust; Magstrat, magnetostratigraphic; SQA, Southern Qiulitage Anticline; YKA, Yaken Anticline; YQA, Yiqikelike Anticline.

Table 2
Summary of Initiation Ages of Structures Within the Eastern Kuqa Fold-And-Thrust Belt

Structures	Initiation age (Ma)	Method of age determination	Growth strata	References
Northern Monocline Belt				
South Tian Shan thrust fault	42–36	(U-Th)/He and apatite fission track	\	Du et al. (2007); Chang et al. (2017); Yu et al. (2014)
Jiesidelike anticline	~23.3	Growth strata	N_1j-Q_1x	H. Lu et al. (2010)
Biyoulebaoguzi anticline	22–15.7	(U-Th)/He	\	Yu et al. (2014)
Kelasu–Yiqikelike Structural Belt				
Kelasu–Yiqikelike thrust (KBT)	22–16	Apatite fission track	\	Yu et al. (2014)
Kumugeliemu anticline	>13	Unconformities and growth strata	N_1j-Q_1x	This study; X. Wang et al. (2011)
Bashijiqike anticline	>13	Growth strata	N_1j-Q_1x	This study
Yiqikelike anticline	~13	Magnetostratigraphy, growth strata	N_1k-Q_1x	T. Zhang et al. (2014)
Kasangtuokai anticline	13–9.8	Growth strata	N_1k-Q_1x	This study
Qiulitage Structural Belt				
Kuqatawu anticline	~6.5	Magnetostratigraphy, growth strata	N_2k-Q_1x	This study; Sun et al. (2009)
Eastern Qiulitage anticline	~6.5	Magnetostratigraphy, growth strata	N_2k-Q_1x	T. Zhang et al. (2014)
Front Fold Belt				
Yaken anticline	~5.5	Growth strata	N_2k-Q_1x	This study; Hubert-Ferrari et al. (2007)
Kalayuergun anticline	~5.3	Magnetostratigraphy, growth strata	N_2k-Q_1x	Z. Zhang et al. (2018); Gao et al. (2020)

5.2.2. Control Factors for the Basinward Propagation Process

Numerical and sandbox modeling of fold-thrust wedges indicates that the outward propagation of thrust-related deformation is cyclical, and basically influenced by the ratio of internal rock strength to basal décollement strength and the magnitude of surface erosion or sedimentation (Dahlen et al., 1988; Davis et al., 1983; Fillon et al., 2013; Graveleau & Dominguez, 2008; Hilley et al., 2004; McQuarrie et al., 2008). In the Kuqa FTB, major control factors include (a) distribution of décollements and (b) syntectonic sedimentation as detailed below.

In the early propagation stage of the Kuqa FTB, basinward propagation is characterized by sequential development of the STST, KYT and other deep basement-involved faults during ~42 to ~16 Ma (Figures 11 and 13a). These thrust faults developed in the Paleozoic basement rocks that are previously deformed, metamorphic, or plutonic rocks from prior tectonism (Laborde et al., 2019), lacking subhorizontal, weak lithological layers as regional décollements (Figures 4 and 5). During thrusting, as basement rocks and sedimentary cover rocks transformed upward to the ground, the deformed hanging wall strata results in the formation of synthetic or antithetic thick-skinned structures (Figures 7–9). In this case, the deformation front migrates only when new or pre-existing faults cut upward through the basement and sedimentary cover rocks (Parker & Pearson, 2021; Pfiffner, 2017). Commonly, compared to thrusting along subhorizontal regional décollements, which is energetically advantageous, propagation through thrust faults in basement rocks with limited or no décollement is slow (Heermance et al., 2008; Hilley et al., 2005; Pfiffner, 2006), which could partly explain the early low propagation rate of the Kuqa FTB (>1–1.4 mm/yr, Figures 12 and 13). After a long, slow basinward propagation process within the hinterland, the migration rate of the deformation front significantly accelerated during the middle Miocene (ca. 12 Ma, Figure 12a). This period coincides with relatively high sedimentation rates (>0.3–0.4 mm/yr, Figure 12c), leading to over ~4 km thick, well-bedded, syntectonic sedimentation strata (i.e., fluvial and alluvial sandstone and mudstone in Kangcun and Kuqa formation) above plastic gypsum salt layers in Kumugeliemu and Jidike formations (Figures 4–6). Analog models indicate that the overburden thickness, whether pre-tectonic or syntectonic, significantly influences the deformation style within FTBs, such as the fault geometry, number and spacing of the resulting structures (Barrier et al., 2013; Bonini, 2001; Fillon et al., 2013; Mugnier et al., 1997). This thicker overburden could also facilitate the development of the thin-skinned thrusting and folding (Figure 13b) along

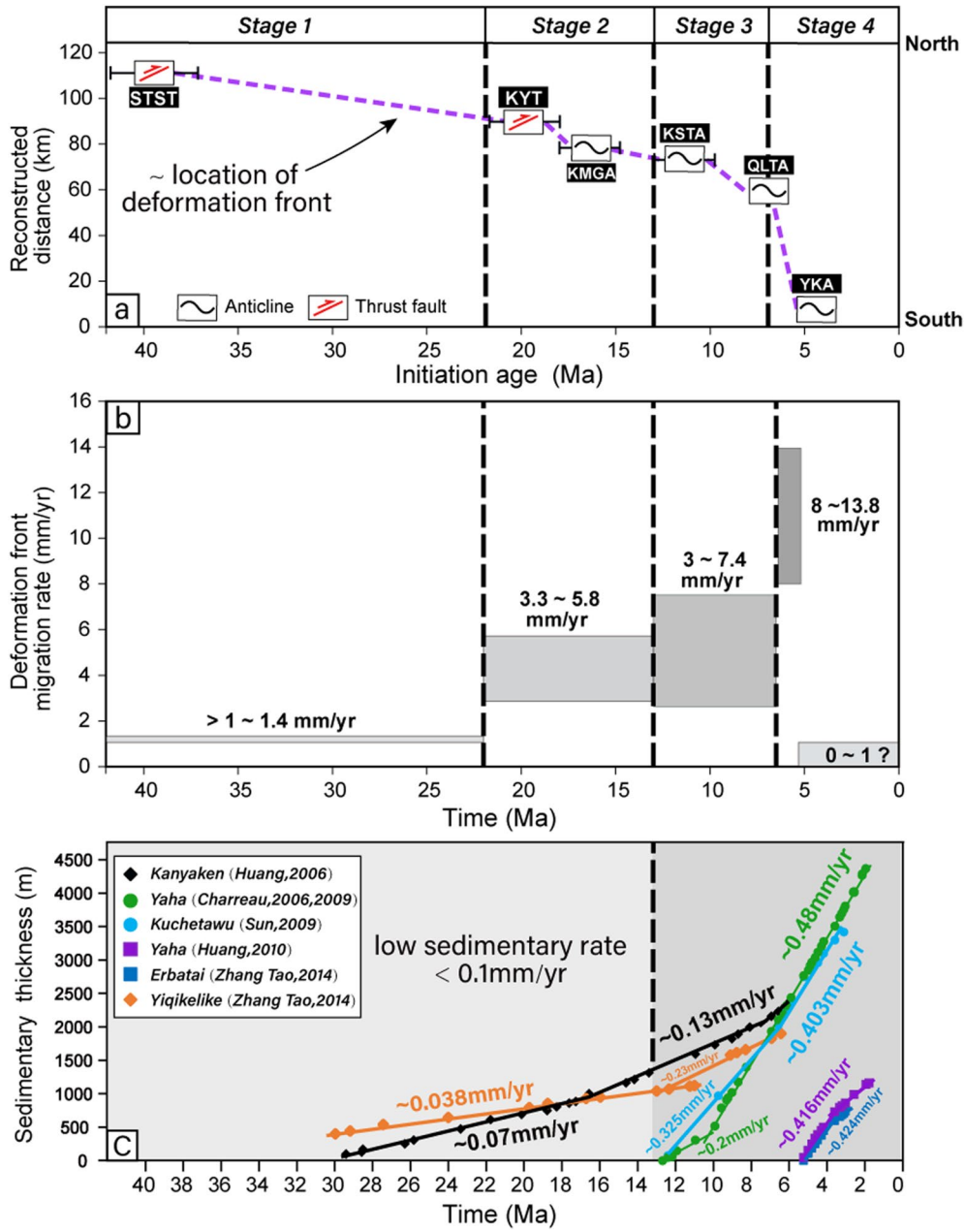

Figure 12. Initiation ages and deformation front migration rates for the eastern Kuqa fold-and-thrust belt (FTB). (a) Boxes with abbreviated locations denote dominant features (thrusts and/or folds) for each structural belt, indicating initiation ages of different structures from the margin of the Tian Shan to the foreland. KMGA, Kumugeliemu Anticline; KSA, Kasangtuokai Anticline; KYT, Kelasu-Yiqikelike Thrust; QLTA, Qiulitage Anticline; STST, South Tian Shan Thrust; YKA, Yaken Anticline. (b) The plot shows variable rates (shaded zones) at which the deformation front migrated basinward within the Kuqa FTB. (c) Sedimentation rates were calculated based on magnetostratigraphic ages and stratigraphic thickness from paleomagnetic sections within the Eastern Kuqa FTB (see location in Figure 2).

both (a) gypsum-salt layers within the Paleocene-Eocene Kumugelimu Formation (E_{1-2} km) or the Early Miocene Jidike Formation (N_1j), and (b) subsalt Jurassic décollement (mainly coals and shales), which is confirmed by recent sandbox modeling of the Kuqa FTB (Pla et al., 2019), and previous simulations of the salt tectonics (Ge et al., 1997; Vendeville, 2005). During this propagation stage, the deformation front mainly migrated along the subhorizontal salt décollement, resulting in high propagation rates (8–13.8 mm/yr, Figure 12b).

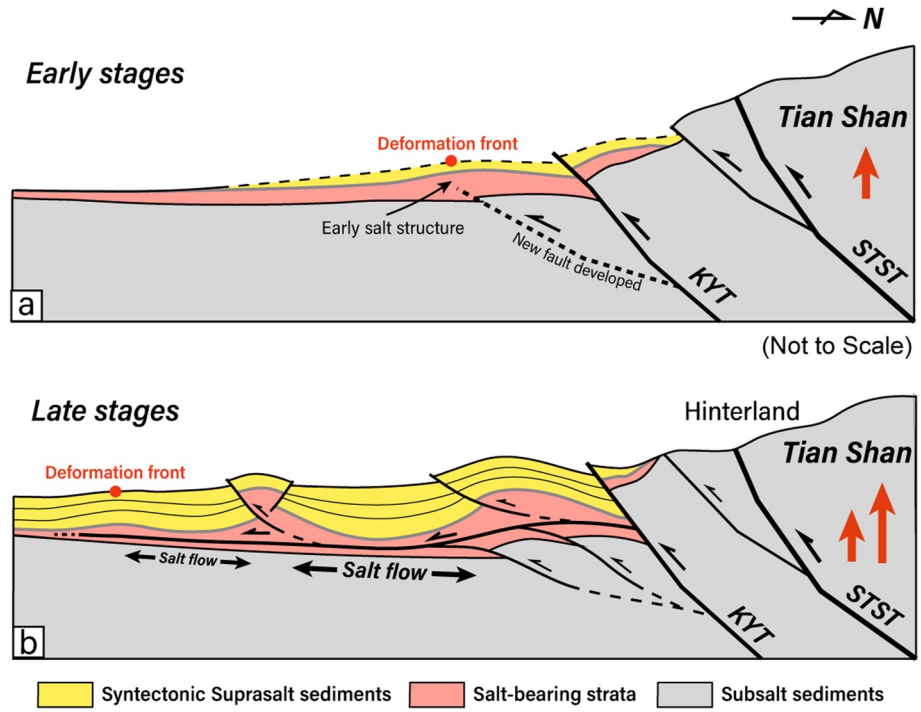

Figure 13. Schematic illustration showing changes in dominant structures during the development of the Kuqa fold-and-thrust belt (FTB). (a) Thick-skinned tectonics dominated the early development of the Kuqa FTB. The deformation front is migrated by new faults rupturing upward through the basement. KYT, Kelasu-Yiqikelike Thrust; STST, South Tian Shan Thrust. (b) Thin-skinned tectonics dominated the late development of the Kuqa FTB. Shortening propagated along plastic gypsum salt layers.

5.3. Implications for the Outward Growth of the Tian Shan

The long-term outward growth of an orogenic wedge is mainly controlled by the interaction among crustal shortening, accretion and erosion (Decelles & Decelles, 2001; Whipple & Meade, 2006). Generally, crustal shortening-driven basinward propagation and erosion-driven retreat are the two competing factors in controlling the migration of orogenic front (Avouac, 2003; McQuarrie et al., 2008; Simoes & Avouac, 2006). Syn-orogenic sedimentation and the development of FTBs within the orogen-foreland basin system provide key insights into the evolution history of the growing orogens. In the Eastern Tian Shan, thanks to several recent studies, long-term denudation over the whole range is proven to be outpaced by crustal thickening; the current Tian Shan range remains in a transient state of topographic growth with limited denudation driven by the arid climate of Central Asia (Charreau et al., 2017, 2023; Guerit et al., 2016; Jolivet et al., 2014; Puchol et al., 2017). Our results in the Kuqa foreland suggest that the deformation front of the whole thrust belt propagated to the Tarim Basin through a "two-stage" process, which is consistent with the evolution of total shortening rates across the Kuqa FTB (Figures 14c and 14e). Additionally, based on detailed tracing of onlap points with high-resolution seismic profiles, C. Li et al. (2019) found that the basinward progradation of syn-orogenic sediments within the Kuqa foreland also shows a two-stage process over the last 26 Ma. The basinward migration rates of traced onlap points have significantly accelerated from ∼1.6 to ∼14.6 mm/yr after ∼12 Ma (Figure 14d). In the Yaha section (Eastern Qiliutage anticline, Kuqa FTB), progradation rates over the last ∼10 Ma were directly constrained by gravel wedges within the Xiyu formation (Charreau et al., 2009). Results indicate that progradation rates were stable, on the order of ∼2 mm/yr during the last ∼10 Ma. Although no older gravel wedges have been found in the Kuqa region to further constrain the progradation rate during the earlier period from ∼20 to ∼10 Ma. Given that the syn-tectonic sedimentation rates during this period are lower than 0.1 mm/yr (Figure 12c), we suspect that the progradation rate in the early stage can be very low. In general, our study of the basinward deformation propagation, together with previous analysis of crustal shortening and sediment progradation, all indicate that the basinward growth of the southern Tian Shan wedge in the Kuqa foreland is characterized by a "two-stage"

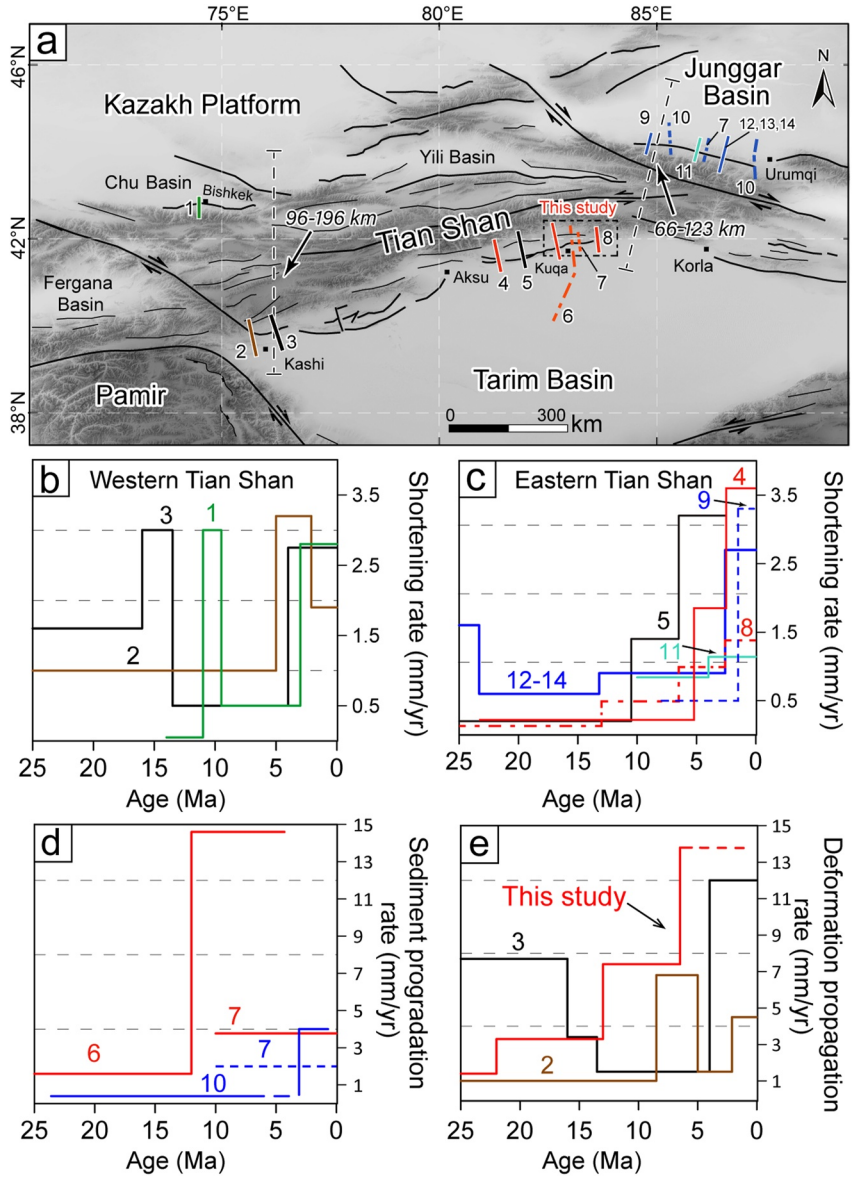

Figure 14. Late Cenozoic shortening, basinward deformation propagation, and sediment progradation rates in the Tian Shan foreland basins. (a) Topographic map of the Tian Shan range with locations of studied cross-sections (1-Bullen et al., 2003; 2-Thompson Jobe et al., 2018; 3-Heermance et al., 2008; 4-S. Li et al., 2012; 5-Izquierdo-Llavall et al., 2018; 6-C. Li et al., 2019; 7-Charreau et al., 2009; 8-T. Zhang et al., 2014; 9-Charreau et al., 2018; 10-C. Li et al., 2022; 11-Charreau et al., 2008; 12-Zhou et al., 2020; 13-Lu et al., 2010; 14-Qiu et al., 2019). Values of crustal shortening across the western and eastern Tian Shan are from Avouac et al. (1993). (b, c) Evolution of total shortening rates of different foreland fold-thrust belts in the western and eastern Tian Shan. (d) Late Cenozoic sediment progradation rates in the northern and southern forelands of the Eastern Tian Shan. Rates are derived from high-resolution seismic lines, drill and magnetostratigraphic data. (e) Basinward propagation rates of the deformation front over the last 25 Myrs.

evolution pattern, with an early (25–12 Ma) slow shortening and propagation, followed by a rapid acceleration after ~12 Ma.

Similar studies have been carried out at the Junggar Basin, Chu Basin in the northern Tian Shan forelands, and Kashi foreland in the southwest Tian Shan (Figure 14a). At the southern Junggar Basin, the basinward growth of the northern Tian Shan orogenic front has been analyzed through gravel wedges that have prograded over the foreland (Charreau et al., 2009; C. Li et al., 2022). The long-term sediment progradation rate in this region is slower than that in Kuqa (Figure 14d). However, at ~3 Ma, both crustal shortening rate and sediment progradation rate

significantly accelerated (Figures 14c and 14d), which may reflect a rapid basinward growth of the northern Tian Shan into the Junggar Basin. Farther west, in the forelands of western Tian Shan, the evolution of both crustal shortening and basinward deformation propagation within the Kashi foreland was investigated by Heermance et al. (2008) and Thompson Jobe et al. (2018). Unlike Kuqa and southern Juggar Basin foreland, results of their studies suggest a "pulsed" evolution of the Kashi FTB, with both shortening and propagation rates accelerated and decelerated several times (Figures 14b and 14d). Additionally, uplift and shortening of the Kyrgyz Range foreland also clearly argue for a pulsed deformation since the late Miocene (Bullen et al., 2003). Collectively, the late Cenozoic outward growth of the Tian Shan is an episodic process, but the propagation patterns and related rates varied in different regions (Figure 14). The main mechanism leading to this spatio-temporal variations is still unclear. In foreland thrust systems, our study in the Kuqa FTB highlights the influence of the distribution of regional décollements, syntectonic sediments. These factors varied in the Tian Shan forelands. For example, along the southern Tian Shan foreland, the main regional décollement varied among the Kashi (Heermance et al., 2007), Kepingtage (Allen et al., 1999) and Kuqa FTBs, which could significantly influence the basinward propagation rates of the thrust wedges. From the view of the whole Tian Shan range, changes in the magnitude of long-term erosion rate, collision or convergence between the Tian Shan and adjacent basins could also contribute to variations in basinward propagation of the orogenic front at different forelands. However, these factors have not been well constrained in the Tian Shan region at present and need further study.

6. Conclusions

In southern Tian Shan foreland, through analysis of three high-resolution and long seismic reflection profiles across the Eastern Kuqa FTB, we observed a westward along-strike increase in total Cenozoic crustal shortening. Within the Kuqa FTB, a telescoped distribution pattern of crustal shortening is also observed in frontal thin-skinned structures above the regional salt décollements, which is consistent with a gradual, basin-ward decrease in shortening, with the maximum across the Kelasu-Yiqikelike structure belt and nearly zero at the tip of the thrust belt. The Cenozoic propagation rates of the deformation front, together with previous analysis of crustal shortening and sediment progradation, all indicate that the basinward growth of the southern Tian Shan wedge in the Kuqa foreland is featured a "two-stage" evolution pattern, with an early (25-12 Ma) slow shortening and propagation, followed by a rapid acceleration after ~12 Ma.

Conflict of Interest

The authors declare no conflicts of interest relevant to this study.

Data Availability Statement

The original data supporting this research are available in Figures 4–6, Figure S1, and Table S1 in Supporting Information S1. All of these high-resolution figures and supporting information can be found online via Zenodo (https://doi.org/10.5281/zenodo.6578624). Reconstruction of cross sections and related shortening calculations are based on the *StructureSolver™* software (Alan & Mary, 2019), available at https://www.structuresolver.com/.

Acknowledgments
This work is supported by the National Key Research and Development Program of China (Grants 2019YFC0605501 and 2022YFC3003704), National Natural Science Foundation of China (Grants U22B6002, 41720104003, 51988101, 41941016, and 41972227). We appreciate the support from the Tarim Oilfield Company, PetroChina. Many thanks to insightful and detailed comments by Profs. Xiubin Lin and Hongdan Deng during the manuscript preparation. We also thank the Editors Dr. Marc Jolivet, Dr. Josep Anton Muñoz and an anonymous reviewer for their constructive comments that improved our manuscript, and thank Alan G. Nunns for permission to use *StructureSolver™* software in the School of Earth Sciences, Zhejiang University.

References

Abdrakhmatov, K. Y., Aldazhanov, S. A., Hager, B. H., Hamburger, M. W., Herring, T. A., Kalabaev, K. B., et al. (1996). Relatively recent construction of the Tien Shan inferred from GPS measurements of present-day crustal deformation rates. *Nature*, *384*(6608), 450–453. https://doi.org/10.1038/384450a0

Abdulhameed, S., Ratschbacher, L., Jonckheere, R., Gągała, Ł., Enkelmann, E., Käßner, A., et al. (2020). Tajik basin and southwestern Tian Shan, Northwestern India-Asia Collision Zone: 2. Timing of basin inversion, Tian Shan mountain building, and relation to Pamir-Plateau advance and deep India-Asia indentation. *Tectonics*, *39*(5), e2019TC005873. https://doi.org/10.1029/2019tc005873

Adeoti, B., & Webb, A. A. G. (2022). Geomorphology of contractional salt tectonics along the Kuqa fold-thrust belt, northwestern China: Testing pre-kinematic diapir versus source-fed thrust and detachment fold models. *Journal of Structural Geology*, *161*, 104638. https://doi.org/10.1016/j.jsg.2022.104638

Alan, N., & Mary, R. (2019). StructureSolver [software]. StructureSolver LLC. Retrieved from https://www.structuresolver.com/

Allen, M. B., Vincent, S. J., & Wheeler, P. J. (1999). Late Cenozoic tectonics of the Kepingtage thrust zone: Interactions of the Tien Shan and Tarim Basin, northwest China. *Tectonics*, *18*(4), 639–654. https://doi.org/10.1029/1999tc900019

Avouac, J.-P. (2003). Mountain building, erosion, and the seismic cycle in the Nepal Himalaya. *Advances in Geophysics*, *46*, 1–80. https://doi.org/10.1016/S0065-2687(03)46001-9

Avouac, J.-P., & Tapponnier, P. (1993). Kinematic model of active deformation in central Asia. *Geophysical Research Letters*, *20*(10), 895–898. https://doi.org/10.1029/93gl00128

Avouac, J. P., Tapponnier, P., Bai, M., You, H., & Wang, G. (1993). Active thrusting and folding along the northern Tien Shan and Late Cenozoic rotation of the Tarim relative to Dzungaria and Kazakhstan. *Journal of Geophysical Research*, *98*(B4), 6755–6804. https://doi.org/10.1029/92jb01963

Barrier, L., Nalpas, T., Gapais, D., & Proust, J.-N. (2013). Impact of synkinematic sedimentation on the geometry and dynamics of compressive growth structures: Insights from analogue modelling. *Tectonophysics*, *608*, 737–752. https://doi.org/10.1016/j.tecto.2013.08.005

Bonini, M. (2001). Passive roof thrusting and forelandward fold propagation in scaled brittle-ductile physical models of thrust wedges. *Journal of Geophysical Research*, *106*(B2), 2291–2311. https://doi.org/10.1029/2000jb900310

Boyer, S. E., & Elliott, D. (1982). Thrust systems. *AAPG Bulletin*, *66*(9), 1196–1230. https://doi.org/10.1306/03b5a77d-16d1-11d7-8645000102c1865d

Bullen, M. E., Burbank, D. W., & Garver, J. I. (2003). Building the Northern Tien Shan: Integrated thermal, structural, and topographic Constraints. *The Journal of Geology*, *111*(2), 149–165. https://doi.org/10.1086/345840

Burchfiel, B. C., Brown, E. T., Qidong, D., Xianyue, F., Jun, L., Molnar, P., et al. (1999). Crustal shortening on the margins of the Tien Shan, Xinjiang, China. *International Geology Review*, *41*(8), 665–700. https://doi.org/10.1080/00206819909465164

Chamberlin, R. T. (1910). The Appalachian folds of central Pennsylvania. *The Journal of Geology*, *18*(3), 228–251. https://doi.org/10.1086/621722

Chang, J., Li, D., Min, K., Qiu, N., Xiao, Y., Wu, H., & Liu, N. (2019). Cenozoic deformation of the Kalpin fold-and-thrust belt, southern Chinese Tian Shan: New insights from low-T thermochronology and sandbox modeling. *Tectonophysics*, *766*, 416–432. https://doi.org/10.1016/j.tecto.2019.06.018

Chang, J., Tian, Y., & Qiu, N. (2017). Mid-Late Miocene deformation of the northern Kuqa fold-and-thrust belt (southern Chinese Tian Shan): An apatite (U-Th-Sm)/He study. *Tectonophysics*, *694*, 101–113. https://doi.org/10.1016/j.tecto.2016.12.003

Charreau, J., Avouac, J.-P., Chen, Y., Dominguez, S., & Gilder, S. (2008). Miocene to present kinematics of fault-bend folding across the Huergu-osi anticline, northern Tianshan (China), derived from structural, seismic, and magnetostratigraphic data. *Geology*, *36*(11), 871–874. https://doi.org/10.1130/g25073a.1

Charreau, J., Blard, P.-H., Lavé, J., Dominguez, S., & Li, W. S. (2023). Unsteady topography in the eastern Tianshan due to imbalance between denudation and crustal thickening. *Tectonophysics*, *848*, 229702. https://doi.org/10.1016/j.tecto.2022.229702

Charreau, J., Gilder, S., Chen, Y., Dominguez, S., Avouac, J.-P., Sen, S., et al. (2006). Magnetostratigraphy of the Yaha section, Tarim Basin (China): 11 Ma acceleration in erosion and uplift of the Tian Shan mountains. *Geology*, *34*(3), 181–184. https://doi.org/10.1130/g22106.1

Charreau, J., Gumiaux, C., Avouac, J., Augier, R., Chen, Y., Barrier, L., et al. (2009). The Neogene Xiyu Formation, a diachronous prograding gravel wedge at front of the Tianshan: Climatic and tectonic implications. *Earth and Planetary Science Letters*, *287*(3), 298–310. https://doi.org/10.1016/j.epsl.2009.07.035

Charreau, J., Saint-Carlier, D., Dominguez, S., Lavé, J., Blard, P.-H., Avouac, J.-P., et al. (2017). Denudation outpaced by crustal thickening in the eastern Tianshan. *Earth and Planetary Science Letters*, *479*, 179–191. https://doi.org/10.1016/j.epsl.2017.09.025

Charreau, J., Saintcarlier, D., Lave, J., Dominguez, S., Blard, P., Avouac, J., et al. (2018). Late Pleistocene acceleration of deformation across the northern Tianshan piedmont (China) evidenced from the morpho-tectonic evolution of the Dushanzi anticline. *Tectonophysics*, *730*, 132–140. https://doi.org/10.1016/j.tecto.2018.02.016

Charreau, J., Sartegou, A., Saintcarlier, D., Lave, J., Blard, P., Dominguez, S., et al. (2020). Late Miocene to Quaternary slip history across the Qiulitag anticline in the southern Tianshan piedmont. *Terra Nova*, *32*(1), 89–96. https://doi.org/10.1111/ter.12439

Daëron, M., Avouac, J. P., & Charreau, J. (2007). Modeling the shortening history of a fault tip fold using structural and geomorphic records of deformation. *Journal of Geophysical Research*, *112*(B3), B03S13. https://doi.org/10.1029/2006JB004460

Dahlen, F. A., Suppe, J., Clark, S. P., Jr., Burchfiel, B. C., & Suppe, J. (1988). Mechanics, growth, and erosion of mountain belts. In *Processes in continental lithospheric deformation* (Vol. 218). Geological Society of America. https://doi.org/10.1130/SPE218-p161

Dahlstrom, C. D. A. (1969). Balanced cross sections. *Canadian Journal of Earth Sciences*, *6*(4), 743–757. https://doi.org/10.1139/e69-069

Davis, D., Suppe, J., & Dahlen, F. A. (1983). Mechanics of fold-and-thrust belts and accretionary wedges. *Journal of Geophysical Research*, *88*(B2), 1153–1172. https://doi.org/10.1029/JB088iB02p01153

Decelles, P. G., & Decelles, P. C. (2001). Rates of shortening, propagation, underthrusting, and flexural wave migration in continental orogenic systems. *Geology*, *29*(2), 135. https://doi.org/10.1130/0091-7613(2001)029%3C0135:ROSPUA%3E2.0.CO;2

Delcaillau, B., Graveleau, F., Saint Carlier, D., Rao, G., Le Béon, M., Charreau, J., & Nexer, M. (2021). Geomorphic analysis of active fold growth and landscape evolution in the central Qiulitage fold belt, southern Tian Shan, China. *Geomorphology*, *398*, 108063. https://doi.org/10.1016/j.geomorph.2021.108063

Du, Z., Wang, Q.-C., & Zhou, X. (2007). Mesozoic and Cenozoic uplifting history of the Kuqa-South Tianshan Basin-Mountain System from the evidence of apatite fission track analysis. *Acta Petrologica et Mineralogica*, *26*(5), 399–408.

Dumitru, T. A., Zhou, D., Chang, E. Z., Graham, S. A., Hendrix, M. S., Sobel, E. R., & Carroll, A. R. (2001). Uplift, exhumation, and deformation in the Chinese Tian Shan. *Geological Society of America Memoir*, *194*, 71–99. https://doi.org/10.1130/0-8137-1194-0.71

Epard, J.-L., & Groshong, R. H., Jr. (1993). Excess area and depth to detachment. *AAPG Bulletin*, *77*(8), 1291–1302. https://doi.org/10.1306/BDFF8E66-1718-11D7-8645000102C1865D

Fillon, C., Huismans, R. S., & Der Beek, P. V. (2013). Syntectonic sedimentation effects on the growth of fold-and-thrust belts. *Geology*, *41*(1), 83–86. https://doi.org/10.1130/G33531.1

Gao, L., Rao, G., Tang, P., Qiu, J., Peng, Z., Pei, Y., et al. (2020). Structural development at the leading edge of the salt-bearing Kuqa fold-and-thrust belt, southern Tian Shan, NW China. *Journal of Structural Geology*, *140*, 104184. https://doi.org/10.1016/j.jsg.2020.104184

Ge, H., Jackson, M. P., & Vendeville, B. C. (1997). Kinematics and dynamics of salt tectonics driven by progradation. *AAPG Bulletin*, *81*(3), 398–423. https://doi.org/10.1306/522B4361-1727-11D7-8645000102C1865D

Ghani, H., Sobel, E. R., Zeilinger, G., Glodny, J., Irum, I., & Sajid, M. (2021). Spatio-temporal structural evolution of the Kohat fold and thrust belt of Pakistan. *Journal of Structural Geology*, *145*, 104310. https://doi.org/10.1016/j.jsg.2021.104310

Gonzalez-Mieres, R., & Suppe, J. (2006). Relief and shortening in detachment folds. *Journal of Structural Geology*, *28*(10), 1785–1807. https://doi.org/10.1016/j.jsg.2006.07.001

Gonzalez-Mieres, R., & Suppe, J. (2011). Shortening histories in active detachment folds based on area-of-relief methods. https://doi.org/10.1306/13251332M943428

Goode, J. K., Burbank, D. W., & Ormukov, C. (2014). Pliocene-Pleistocene initiation, style, and sequencing of deformation in the central Tien Shan. *Tectonics*, *33*(4), 464–484. https://doi.org/10.1002/2013TC003394

Graveleau, F., & Dominguez, S. (2008). Analogue modelling of the interaction between tectonics, erosion and sedimentation in foreland thrust belts. *Comptes Rendus Geoscience*, *340*(5), 324–333. https://doi.org/10.1016/j.crte.2008.01.005

Groshong, R. H., Jr. (2015). Quality control and risk assessment of seismic profiles using area-depth-strain analysis. *Interpretation*, *3*(4), SAA1–SAA15. https://doi.org/10.1190/INT-2015-0010.1

Guerit, L., Barrier, L., Jolivet, M., Fu, B., & Metivier, F. (2016). Denudation intensity and control in the Chinese Tian Shan: New constraints from mass balance on catchment-alluvial fan systems. *Earth Surface Processes and Landforms*, *41*(8), 1088–1106. https://doi.org/10.1002/esp.3890

Heermance, R. V., Chen, J., Burbank, D. W., & Miao, J. (2008). Temporal constraints and pulsed Late Cenozoic deformation during the structural disruption of the active Kashi foreland, northwest China. *Tectonics*, *27*(6), TC6012. https://doi.org/10.1029/2007TC002226

Heermance, R. V., Chen, J., Burbank, D. W., & Wang, C. (2007). Chronology and tectonic controls of Late Tertiary deposition in the southwestern Tian Shan foreland, NW China. *Basin Research*, *19*(4), 599–632. https://doi.org/10.1111/j.1365-2117.2007.00339.x

Hendrix, M. S., Graham, S. A., Carroll, A. R., Sobel, E. R., McKNIGHT, C. L., Schulein, B. J., & Wang, Z. (1992). Sedimentary record and climatic implications of recurrent deformation in the Tian Shan: Evidence from Mesozoic strata of the north Tarim, south Junggar, and Turpan basins, northwest China. *Geological Society of America Bulletin*, *104*(1), 53–79. https://doi.org/10.1130/0016-7606(1992)104%3C0053:SRACIO%3E2.3.CO;2

Hilley, G. E., Blisniuk, P. M., & Strecker, M. R. (2005). Mechanics and erosion of basement-cored uplift provinces. *Journal of Geophysical Research*, *110*(B12), B12409. https://doi.org/10.1029/2005JB003704

Hilley, G. E., Strecker, M. R., & Ramos, V. A. (2004). Growth and erosion of fold-and-thrust belts with an application to the Aconcagua fold-and-thrust belt, Argentina. *Journal of Geophysical Research*, *109*(B1), 19. https://doi.org/10.1029/2002JB002282

Hossack, J. R. (1979). The use of balanced cross-sections in the calculation of orogenic contraction: A review. *Journal of the Geological Society*, *136*(6), 705–711. https://doi.org/10.1144/gsjgs.136.6.0705

Huang, B., Piper, J., Peng, S., Liu, T., Li, Z., Wang, Q., & Zhu, R. (2006). Magnetostratigraphic study of the Kuche depression, Tarim Basin, and Cenozoic uplift of the Tian Shan range, Western China. *Earth and Planetary Science Letters*, *251*(3–4), 346–364. https://doi.org/10.1016/j.epsl.2006.09.020

Huang, K., Wu, L., Zhang, J., Zhang, Y., Xiao, A., Lin, X., et al. (2020). Structural coupling between the Qiman Tagh and the Qaidam basin, northern Tibetan Plateau: A perspective from the Yingxiong range by integrating field mapping, seismic imaging, and analogue modeling. *Tectonics*, *39*(12), e2020TC006287. https://doi.org/10.1029/2020tc006287

Hubert-ferrari, A., Suppe, J., Gonzalezmieres, R., & Wang, X. (2007). Mechanisms of active folding of the landscape (southern Tian Shan, China). *Journal of Geophysical Research*, *112*(B3), B03S09. https://doi.org/10.1029/2006JB004362

Izquierdo-Llavall, E., Roca, E., Xie, H., Pla, O., Muñoz, J. A., Rowan, M. G., et al. (2018). Influence of overlapping décollements, syntectonic sedimentation, and structural inheritance in the evolution of a contractional system: The central Kuqa fold-and-thrust belt (Tian Shan Mountains, NW China). *Tectonics*, *37*(8), 2608–2632. https://doi.org/10.1029/2017TC004928

Jolivet, M., Barrier, L., Dominguez, S., Guerit, L., Heilbronn, G., & Fu, B. (2014). Unbalanced sediment budgets in the catchment–alluvial fan system of the Kuitun River (northern Tian Shan, China): Implications for mass-balance estimates, denudation and sedimentation rates in orogenic systems. *Geomorphology*, *214*, 168–182. https://doi.org/10.1016/j.geomorph.2014.01.024

Laborde, A., Barrier, L., Simoes, M., Li, H., Coudroy, T., Der Woerd, J. V., & Tapponnier, P. (2019). Cenozoic deformation of the Tarim Basin and surrounding ranges (Xinjiang, China): A regional overview. *Earth-Science Reviews*, *197*, 102891. https://doi.org/10.1016/j.earscirev.2019.102891

Li, C., Wang, S., Li, Y., Chen, Y., Sinclair, H., Wei, D., et al. (2022). Growth of the Tian Shan drives migration of the Conglomerate-sandstone transition in the southern Junggar Foreland Basin. *Geophysical Research Letters*, *49*(4), e2021GL097545. https://doi.org/10.1029/2021gl097545

Li, C., Wang, S., & Wang, L. (2019). Tectonostratigraphic history of the southern Tian Shan, western China, from seismic reflection profiling. *Journal of Asian Earth Sciences*, *172*, 101–114. https://doi.org/10.1016/j.jseaes.2018.08.017

Li, S., Tang, P., & Rao, G. (2013). Cenozoic deformation characteristics and controlling factors of Kalayuergun structural belt, Kuqa fold and thrust belt, southern Tianshan [in Chinese with English abstract]. *Earth Science Journal of China University of Geosciences*, *38*(4), 859–869. https://doi.org/10.3799/dqkx.2013.084

Li, S., Wang, X., & Suppe, J. (2012). Compressional salt tectonics and synkinematic strata of the western Kuqa foreland basin, southern Tian Shan, China. *Basin Research*, *24*(4), 475–497. https://doi.org/10.1111/j.1365-2117.2011.00531.x

Lu, H., Burbank, D. W., Li, Y., & Liu, Y. (2010). Late Cenozoic structural and stratigraphic evolution of the northern Chinese Tian Shan foreland. *Basin Research*, *22*(3), 249–269. https://doi.org/10.1111/j.1365-2117.2009.00412.x

Lu, H., Li, B., Wu, D., Zhao, J., Zheng, X., Xiong, J., & Li, Y. (2019). Spatiotemporal patterns of the Late Quaternary deformation across the northern Chinese Tian Shan foreland. *Earth-Science Reviews*, *194*, 19–37. https://doi.org/10.1016/j.earscirev.2019.04.026

Lu, L., Sun, J., Zhang, Z., Jia, Y., Li, T., Li, C., & Cao, M. (2019). Cenozoic deformation and crustal shortening in the foreland of southern Tian Shan, NW China, as a response to the India-Asia collision. *Journal of Asian Earth Sciences*, *183*, 103960. https://doi.org/10.1016/j.jseaes.2019.103960

McQuarrie, N., Ehlers, T. A., Barnes, J. B., & Meade, B. (2008). Temporal variation in climate and tectonic coupling in the central Andes. *Geology*, *36*(12), 999–1002. https://doi.org/10.1130/G25124A.1

Meigs, A. (1997). Sequential development of selected Pyrenean thrust faults. *Journal of Structural Geology*, *19*(3–4), 481–502. https://doi.org/10.1016/S0191-8141(96)00096-X

Miao, Y., Herrmann, M., Wu, F., Yan, X., & Yang, S. (2012). What controlled Mid–Late Miocene long-term aridification in Central Asia?—Global cooling or Tibetan Plateau uplift: A review. *Earth-Science Reviews*, *112*(3), 155–172. https://doi.org/10.1016/j.earscirev.2012.02.003

Molnar, P., & Tapponnier, P. (1975). Cenozoic tectonics of Asia: Effects of a continental collision. *Science*, *189*(4201), 419–426. https://doi.org/10.1126/science.189.4201.419

Mugnier, J., Baby, P., Colletta, B., Vinour, P., Bale, P., & Leturmy, P. (1997). Thrust geometry controlled by erosion and sedimentation: A view from analogue models. *Geology*, *25*(5), 427–430. https://doi.org/10.1130/0091-7613(1997)025%3C0427:TGCBEA%3E2.3.CO;2

Neng, Y., Xie, H., Yin, H., Li, Y., & Wang, W. (2018). Effect of basement structure and salt tectonics on deformation styles along strike: An example from the Kuqa fold–thrust belt, West China. *Tectonophysics*, *730*, 114–131. https://doi.org/10.1016/j.tecto.2018.02.006

Parker, S. D., & Pearson, D. M. (2021). Pre-thrusting stratigraphic control on the transition from a thin- to thick-skinned structural style: An example from the double-decker Idaho-Montana fold-thrust belt. *Tectonics*, *40*(5), e2020TC006429. https://doi.org/10.1029/2020tc006429

Pfiffner, O. A. (2006). Thick-skinned and thin-skinned styles of continental contraction. *Special Paper of the Geological Society of America*, *414*(9), 1–10. https://doi.org/10.1130/2006.2414(09)

Pfiffner, O. A. (2017). Thick-skinned and thin-skinned tectonics: A global perspective. *Geosciences*, *7*(3), 71. https://doi.org/10.20944/preprints201707.0020.v1

Pla, O., Roca, E., Xie, H., Izquierdo-Llavall, E., Muñoz, J. A., Rowan, M. G., et al. (2019). Influence of syntectonic sedimentation and décollement rheology on the geometry and evolution of orogenic wedges: Analog modeling of the Kuqa fold-and-Thrust belt (NW China). *Tectonics*, *38*(8), 2727–2755. https://doi.org/10.1029/2018TC005386

Prud'Homme, C., Scardia, G., Vonhof, H., Guinoiseau, D., Nigmatova, S., Fiebig, J., et al. (2021). Central Asian modulation of Northern Hemisphere moisture transfer over the Late Cenozoic. *Communications Earth & Environment*, *2*(1), 106. https://doi.org/10.1038/s43247-021-00173-z

Puchol, N., Charreau, J., Blard, P., Lave, J., Dominguez, S., Pik, R., et al. (2017). Limited impact of Quaternary glaciations on denudation rates in Central Asia. *Geological Society of America Bulletin*, *129*(3–4), 479–499. https://doi.org/10.1130/B31475.1

Qayyum, M., Spratt, D. A., Dixon, J. M., & Lawrence, R. D. (2015). Displacement transfer from fault-bend to fault-propagation fold geometry: An example from the Himalayan thrust front. *Journal of Structural Geology*, *77*, 260–276. https://doi.org/10.1016/j.jsg.2014.10.010

Qi, J., Lei, G., Li, M., Xie, H., & Yang, S. (2009). Contractional structure model of the Transition belt between Kuche depression and south Tianshan uplift. *Earth Science Frontiers*, *16*(3), 120–128. https://doi.org/10.1016/S1872-5791(08)60089-5

Qiao, Q. Q., Huang, B. C., Biggin, A. J., & Piper, J. D. A. (2017). Late Cenozoic evolution in the Pamir-Tian Shan convergence: New chronological constraints from the magnetostratigraphic record of the southwestern Tianshan foreland basin (Ulugqat area). *Tectonophysics*, *717*, 51–64. https://doi.org/10.1016/j.tecto.2017.07.013

Qiu, J., Rao, G., Wang, X., Yang, D., & Xiao, L. (2019). Effects of fault slip distribution on the geometry and kinematics of the southern Junggar fold-and-thrust belt, northern Tian Shan. *Tectonophysics*, *772*, 228–209. https://doi.org/10.1016/j.tecto.2019.228209

Reigber, C., Michel, G., Galas, R., Angermann, D., Klotz, J., Chen, J., et al. (2001). New space geodetic constraints on the distribution of deformation in Central Asia. *Earth and Planetary Science Letters*, *191*(1–2), 157–165. https://doi.org/10.1016/S0012-821X(01)00414-9

Saint-carlier, D., Charreau, J., Lave, J., Blard, P., Dominguez, S., Avouac, J., et al. (2016). Major temporal variations in shortening rate absorbed along a large active fold of the southeastern Tianshan piedmont (China). *Earth and Planetary Science Letters*, *434*, 333–348. https://doi.org/10.1016/j.epsl.2015.11.041

Scharer, K. M., Burbank, D. W., Chen, J., Weldon, R. J., Rubin, C., Zhao, R., & Shen, J. (2004). Detachment folding in the southwestern Tian Shan–Tarim foreland, China: Shortening estimates and rates. *Journal of Structural Geology*, *26*(11), 2119–2137. https://doi.org/10.1016/j.jsg.2004.02.016

Simoes, M., & Avouac, J. P. (2006). Investigating the kinematics of mountain building in Taiwan from the spatiotemporal evolution of the foreland basin and western foothills. *Journal of Geophysical Research*, *111*(B10), B10401. https://doi.org/10.1029/2005jb004209

Sobel, E., Chen, J., & Heermance, R. (2006). Late Oligocene–early Miocene initiation of shortening in the southwestern Chinese Tian Shan: Implications for Neogene shortening rate variations. *Earth and Planetary Science Letters*, *247*(1–2), 70–81. https://doi.org/10.1016/j.epsl.2006.03.048

Sun, J., Gong, Z., Tian, Z., Jia, Y., & Windley, B. (2015). Late Miocene stepwise aridification in the Asian interior and the interplay between tectonics and climate. *Palaeogeography, Palaeoclimatology, Palaeoecology*, *421*, 48–59. https://doi.org/10.1016/j.palaeo.2015.01.001

Sun, J., Li, Y., Zhang, Z., & Fu, B. (2009). Magnetostratigraphic data on Neogene growth folding in the foreland basin of the southern Tianshan Mountains. *Geology*, *37*(11), 1051–1054. https://doi.org/10.1130/G30278A.1

Tang, P., Rao, G., Li, S., Yu, Y., Pei, Y., Wang, X., et al. (2017). Lateral structural variations and drainage response along the Misikantage anticline in the western Kuqa fold-and-thrust belt, southern Tianshan, NW China. *Tectonophysics*, *721*, 196–210. https://doi.org/10.1016/j.tecto.2017.10.007

Tapponnier, P., & Molnar, P. (1979). Active faulting and Cenozoic tectonics of the Tien Shan, Mongolia, and Baykal regions. *Journal of Geophysical Research*, *84*(B7), 3425–3459. https://doi.org/10.1029/jb084ib07p03425

Thompson, J. A., Burbank, D. W., Li, T., Chen, J., & Bookhagen, B. (2015). Late Miocene northward propagation of the northeast Pamir thrust system, northwest China. *Tectonics*, *34*(3), 510–534. https://doi.org/10.1002/2014tc003690

Thompson Jobe, J. A., Li, T., Bookhagen, B., Chen, J., & Burbank, D. (2018). Dating growth strata and basin fill by combining $^{26}Al/^{10}Be$ burial dating and magnetostratigraphy: Constraining active deformation in the Pamir–Tian Shan convergence zone, NW China. *Lithosphere*, *10*(6), 806–828. https://doi.org/10.1130/l727.1

Tian, Z., Sun, J., Windley, B. F., Zhang, Z., Gong, Z., Lin, X., & Xiao, W. (2016). Cenozoic detachment folding in the southern Tianshan foreland, NW China: Shortening distances and rates. *Journal of Structural Geology*, *84*, 142–161. https://doi.org/10.1016/j.jsg.2016.01.007

Vendeville, B. C. (2005). Salt tectonics driven by sediment progradation: Part I—Mechanics and kinematics. *AAPG Bulletin*, *89*(8), 1071–1079. https://doi.org/10.1306/03310503063

Wang, Q., Zhang, P., Freymueller, J. T., Bilham, R., Larson, K. M., Lai, X., et al. (2001). Present-day crustal deformation in China constrained by global positioning system measurements. *Science*, *294*(5542), 574–577. https://doi.org/10.1126/science.1063647

Wang, W., Yin, H., Jia, D., & Li, C. (2017). A sub-salt structural model of the Kelasu structure in the Kuqa foreland basin, northwest China. *Marine and Petroleum Geology*, *88*, 115–126. https://doi.org/10.1016/j.marpetgeo.2017.08.008

Wang, W., Yin, H., Jia, D., Neng, Y., Zhou, P., Chen, W., et al. (2020). Along-strike structural variation in a salt-influenced fold and thrust belt: Analysis of the Kuqa depression. *Tectonophysics*, *786*, 228456. https://doi.org/10.1016/j.tecto.2020.228456

Wang, X., Suppe, J., Guan, S. W., Hubert-Ferrari, A., & Jia, C. Z. (2011). Cenozoic structure and Tectonic evolution of the Kuqa Foldbelt, southern Tianshan, China. *American Association of Petroleum Geologists Memoir*, *94*(94), 215–243. https://doi.org/10.1306/13251339M94389

Watkins, H., Butler, R. W. H., & Bond, C. E. (2017). Using laterally compatible cross sections to infer fault growth and linkage models in foreland thrust belts. *Journal of Structural Geology*, *96*, 102–117. https://doi.org/10.1016/j.jsg.2017.01.010

Whipple, K. X., & Meade, B. J. (2006). Orogen response to changes in climatic and tectonic forcing. *Earth and Planetary Science Letters*, *243*(1), 218–228. https://doi.org/10.1016/j.epsl.2005.12.022

Wiltschko, D. V., & Groshong, R. H. (2012). The Chamberlin 1910 balanced section: Context, contribution, and critical reassessment. *Journal of Structural Geology*, *41*, 7–23. https://doi.org/10.1016/j.jsg.2012.01.019

Wu, C. Y., Zheng, W. J., Zhang, P. Z., Zhang, Z. Q., Jia, Q. C., Yu, J. X., et al. (2019). Oblique Thrust of the Maidan fault and Late Quaternary Tectonic deformation in the southwestern Tian Shan, Northwestern China. *Tectonics*, *38*(8), 2625–2645. https://doi.org/10.1029/2018tc005248

Wu, Z., Yin, H., Wang, X., Zhao, B., & Jia, D. (2014). Characteristics and deformation mechanism of salt-related structures in the western Kuqa depression, Tarim basin: Insights from scaled sandbox modeling. *Tectonophysics*, *612–613*, 81–96. https://doi.org/10.1016/j.tecto.2013.11.040

Yang, M., Jin, Z., Lu, X., Sun, D., & Zeng, P. (2010). Tectono-sedimentary evolution of Piggy-back basin: Example from Kuqa fold and Thrust belt, Northern Tarim Basin, Northwest China. *Journal of Earth Sciences*, *000*(004), 412–422. https://doi.org/10.1007/s12583-010-0104-2

Yang, S., Li, J., & Wang, Q. (2008). The deformation pattern and fault rate in the Tianshan Mountains inferred from GPS observations. *Science in China Series D: Earth Sciences*, *51*(8), 1064–1080. https://doi.org/10.1007/s11430-008-0090-8

Yang, W., Jianfeng, L. I., Guo, Z., Jolivet, M., & Heilbronn, G. (2017). New apatite fission-Track ages of the Western Kuqa depression: Implications for the Mesozoic–Cenozoic Tectonic evolution of south Tianshan, Xinjiang. *Acta Geologica Sinica-English Edition*, *91*(2), 391–413. https://doi.org/10.1111/1755-6724.13107

Yang, X., Deng, Q., Zhang, P., & Xu, X. (2008). Crustal shortening of major nappe structures on the front margins of the Tianshan [in Chinese with English abstract]. *Seismology and Geology*, *30*(1), 111–131. Retrieved from https://www.dzdz.ac.cn/EN/

Yin, A., Nie, S., Craig, P., Harrison, T. M., Ryerson, F. J., Xianglin, Q., & Geng, Y. (1998). Late Cenozoic tectonic evolution of the southern Chinese Tian Shan. *Tectonics*, *17*(1), 1–27. https://doi.org/10.1029/97tc03140

Yu, S., Chen, W., Evans, N. J., McInnes, B. I. A., Yin, J., Sun, J., et al. (2014). Cenozoic uplift, exhumation and deformation in the north Kuqa Depression, China as constrained by (U–Th)/He thermochronometry. *Tectonophysics*, *630*, 166–182. https://doi.org/10.1016/j.tecto.2014.05.021

Zhang, L., Yang, X., Huang, W., Yang, H., & Li, S. (2021). Fold segment linkage and lateral propagation along the Qiulitage anticline, South Tianshan, NW China. *Geomorphology*, *381*, 107662. https://doi.org/10.1016/j.geomorph.2021.107662

Zhang, T., Fang, X., Song, C., Appel, E., & Wang, Y. (2014). Cenozoic tectonic deformation and uplift of the South Tian Shan: Implications from magnetostratigraphy and balanced cross-section restoration of the Kuqa depression. *Tectonophysics*, *628*, 172–187. https://doi.org/10.1016/j.tecto.2014.04.044

Zhang, Z., Shen, Z., Sun, J., Wang, X., Tian, Z., Pan, X., & Shi, L. (2015). Magnetostratigraphy of the Kelasu section in the Baicheng depression, southern Tian Shan, northwestern China. *Journal of Asian Earth Sciences*, *111*, 492–504. https://doi.org/10.1016/j.jseaes.2015.06.016

Zhang, Z., Sun, J., Lu, L., Tian, S., Cao, M., Su, B., et al. (2019). Late Cenozoic clockwise rotations in the westernmost part of the arcuate Qiulitage fold-and-thrust belt of southern Tian Shan foreland and its tectonic implications. *Tectonics*, *38*(6), 2036–2058. https://doi.org/10.1029/2018TC005172

Zhang, Z., Sun, J., Lu, L., Wang, W., & Li, Y. (2018). Neogene Paleomagnetic study of the Western Baicheng depression: Implications for the intensified deformation of Tian Shan since the Latest Miocene. *Journal of Geophysical Research*, *123*(12), 10–349. https://doi.org/10.1029/2018JB016953

Zhang, Z., Sun, J., Tian, Z., & Gong, Z. (2016). Magnetostratigraphy of syntectonic growth strata and implications for the late Cenozoic deformation in the Baicheng Depression, Southern Tian Shan. *Journal of Asian Earth Sciences*, *118*, 111–124. https://doi.org/10.1016/j.jseaes.2015.12.024

Zhou, Y., Wu, C., Yuan, B., Wang, J., Zhou, T., Wang, Y., & Tang, X. (2020). Cenozoic tectonic patterns and their controls on growth strata in the northern Tianshan fold and thrust belt, northwest China. *Journal of Asian Earth Sciences*, *198*, 104–237. https://doi.org/10.1016/j.jseaes.2020.104237

Zubovich, A. V., Wang, X.-Q., Scherba, Y. G., Schelochkov, G. G., Reilinger, R., Reigber, C., et al. (2010). GPS velocity field for the Tien Shan and surrounding regions. *Tectonics*, *29*(6), TC6014. https://doi.org/10.1029/2010tc002772

Zuza, A. V., Cheng, X., & Yin, A. (2016). Testing models of Tibetan Plateau formation with Cenozoic shortening estimates across the Qilian Shan–Nan Shan thrust belt. *Geosphere*, *12*(2), 501–532. https://doi.org/10.1130/ges01254.1